APPLICATION OF MAGNETORHEOLOGICAL DAMPERS IN MOTORCYCLE REAR SWING ARM SUSPENSION

A thesis presented to the faculty of the Graduate School of
Western Carolina University in partial fulfillment of the
requirements for the degree of Master of Science in Technology.

By:
Benjamin B. Stewart

Advisor:
Dr. Sudhir Kaul
Assistant Professor
Department of Engineering & Technology

Committee Members:
Dr. Aaron Ball, Department of Engineering & Technology
Dr. Robert Adams, Department of Engineering & Technology

October 2015

ACKNOWLEDGEMENTS

I would like to sincerely thank my advisor, Dr. Sudhir Kaul, and my committee members, Dr. Aaron Ball and Dr. Robert Adams. All of them have provided tremendous amounts of support, teaching, encouragement, and assistance over the course of completing this thesis. Without their help and guidance completing this thesis would not have been possible.

I would also like to thank my fellow graduate students, always willing to lend support when needed. Finally I want to thank all of my friends and family who have supported me through this challenging enterprise.

TABLE OF CONTENTS

LIST OF TABLES

LIST OF FIGURES

ABSTRACT

APPLICATION OF MAGNETORHEOLOGICAL DAMPERS IN MOTORCYCLE SWING ARM SUSPENSION

Benjamin B. Stewart, M.S.T.

Western Carolina University (October 2015)

Advisor: Dr. Sudhir Kaul

Magnetorheological (MR) fluid is a smart fluid containing ferrous particles that allow it to change its apparent viscosity in the presence of a magnetic field. Dampers consisting of MR fluids provide a means of active damping by using a current input to an electromagnet to control the damping properties. A swing arm suspension system is unique to two-wheeled vehicles, and links the rear wheel to the frame of the vehicle through a pivot. The swing arm also connects the rear suspension system to the frame. The goal of this study is to experimentally analyze the vibration mitigation capabilities of MR dampers in a (rear) swing arm suspension system in a motorcycle. A set of commercially available MR dampers is used in a fixture that has been developed to represent the rear swing arm system. The dampers are characterized and preliminary mathematical models have been developed to investigate the capability of the damping system. Multiple iterations of testing are performed on the shaker table to evaluate the performance of the damping system at different locations of the frame. Accelerometers are used for this evaluation, and the analysis of the acceleration data is performed in time domain as well as frequency domain. Results indicate that the mitigation in root mean square (RMS) acceleration ranges from 50 to 80% at varying levels of damping. Significant mitigation is

observed at different locations of the fixture that correspond to the rider seat and the position of the foot pegs on a motorcycle. The semi-active behavior of the damper is a critical property that can be used to overcome the constraints of a traditional passive suspension system, where the stiffness and damping is tuned to provide enhanced ride comfort or improved handling. In a passive system, some compromise is necessary between the two competing requirements of ride comfort and handling. The MR damping system could be used to overcome this constraint by exercising direct control over the input current of the electromagnet. The results from this study indicate that an MR damping system would allow the swing arm suspension to adapt so as to provide improved ride comfort as well as enhanced handling.

CHAPTER 1: INTRODUCTION

The suspension system plays a very important role in the operation of the vehicle. A suspension system supports the vehicle's weight, known as the sprung mass, while isolating the main body of the vehicle from any disturbances on the road and allowing the vehicle to maintain constant traction with the road surface [22]. Traditional passive suspension systems are tuned to find an optimum setting where a compromise of ride comfort and handling works best for the type of vehicle that the suspension is being used in. Active and Semi-active dampers are recently being increasingly investigated to overcome many of the constraints that are posed by passive dampers in the design and development of suspension systems. Magnetorheological (MR) dampers are one example of semi-active dampers that have an inherent capability to actively change the damping characteristics so as to maintain optimum performance without requiring a pre-determined compromise between ride comfort and handling. Also, MR dampers require a relatively small amount of energy and the damper can still function as a passive damper in case of a failure.

MR dampers are filled with MR fluid, a smart fluid containing ferrous particles that allow it to change its apparent viscosity in the presence of a magnetic field. This change in apparent viscosity of the fluid is used to change the damping behavior of as the fluid moves through the valves of the damper. These characteristics overcome the constraint posed by passive dampers where low damping is needed to produce a comfortable ride with poor handling, or a high damping is needed to produce improved handling with poor ride comfort.

The currently available semi-active dampers in motorcycle applications are limited to electronically controlled valves inside the fork or the rear shock [18, 14]. This study seeks to

investigate the feasibility of using MR dampers in a motorcycle application, specifically for the rear swing arm suspension. An experimental analysis is conducted by building a fixture and using two commercially available MR dampers. The fixture represents the rear swing arm suspension system and is excited on a shaker table. This thesis seeks to answer the following questions:

1. How does a dual damper rear swing arm suspension system (for motorcycles) equipped with dual MR dampers perform?
2. How can an active control of rear swing arm suspension be set up? Can semi-active control methods such as Skyhook control and Groundhook control (that have been researched for quarter car models [12]) be used? How would the test setup perform if such control methods are implemented?
3. What is the influence of multiple parameters such as excitation frequency, excitation amplitude, input current, etc. on the capability of the damping system to mitigate vibrations transmitted to the rider at multiple locations of the frame? Can these parameters influence handling behavior?

1.1 Scope of Thesis

This thesis evaluates the performance of commercially available MR dampers manufactured by LORD Corporation. The characteristics of the dampers are experimentally established using compression testing at different settings of the damper. These characteristics are then used to develop three possible mathematical models that can be used for predicting the dynamic response of the suspension system.

Multiple iterations of experimental testing and data collection are conducted. The dampers are evaluated under excitation conditions that represent a range of operating frequencies under driving conditions. The shaker table is used to represent the source of excitation. The variables investigated in the experimental study include frequency of vibration, excitation amplitude, and input current to the MR dampers. The choice of the settings is based on constraints of the system, the shaker table, and normal operation conditions for the vehicle in question. Data from the experiments are collected with accelerometers using a c-DAQ system and computer for recording data. The experimental data is then post-processed and analyzed by using MATLAB®.

1.2 Overview of Thesis

This document presents a background of some of the existing designs of motorcycle suspension systems, and discusses the pros and cons of a passive system in comparison with the semi-active and active systems. Chapter 2 consists of a review of the current literature on the application of MR fluids and dampers, and the use of such dampers in motorcycle suspensions.

Chapter 3 discusses the concept of transmissibility and the characteristics of the MR dampers used in this study. The ability of MR dampers to provide semi-active damping that can meet the needs of displacement and force transmissibility is also discussed. Post processing of the data by using the frequency response and filtering is briefly reviewed in this chapter. The swing arm model and three mathematical models that can be used to determine dynamic characteristics are presented. Finally, vibration control and the Skyhook control algorithm simulated for the system are discussed.

In Chapter 4, the test equipment that is used in this study is presented and described. Also included is an extensive illustration of the experimental setup and data collection. A comprehensive overview of the testing and data collection is presented. This chapter also discusses the testing parameters, and all results from the experiment are presented and analyzed.

Chapter 5 concludes this thesis with final remarks and a summary of the findings from the experimental analysis. Possible future work is discussed that can be done as a continuation of this study in order to comprehensively apply MR dampers in rear swing arm suspension systems.

CHAPTER 2: LITERATURE REVIEW

This chapter covers a comprehensive review of current literature on the application of MR dampers in motorcycle suspensions is provided as well as an introduction to MR fluid and dampers.

2.1 Magneto Rheological Fluid and Damping

Magnetorheological (MR) fluid has been around for many years, first brought to light in the 1940s by Jacob Rainbow. However the technology lost popularity until LORD Corporation began using MR fluid in active damper devices in the early 1990s [5]. LORD Corporation, along with other researchers and companies, have been able to implement the use of MR fluid into multiple damping devices, and improve the effectiveness in practical applications by making use of the unique characteristics of the fluid.

MR damping systems are currently available on a variety of high-end luxury and sport automobiles. However, applications of MR damping devices in motorcycles are few and far between with most of the current focus being limited to the technology's applications for cars. This could be attributed to the fact that the market for motorcycles is much smaller than automobiles. It is also possible there is little research in the area is that motorcycle suspension systems play a critical role in the handling stability of a motorcycle, making the design significantly complex.

The concept of reducing vibrations using a damping system has been around for many decades. Suspensions systems are used in a variety of applications including buildings, manufacturing equipment, and automobiles. Traditional suspension systems include a passive

damper that is tuned to meet a specific need over a certain range of vibrations. MR fluid dampers can offer a much greater range of operation and actively change damping capability to mitigate current vibrations in real time [13].

2.1.1 MR Fluid

MR fluid is a smart fluid containing ferrous particles that change their apparent viscosity in the presence of a magnetic field [21]. In the absence of a magnetic field the fluid behaves very similar to free flowing traditional damper fluid. When a magnetic field is introduced in the presence of the MR fluid, micron-sized ferrous particles in the fluid align with the magnetic path to create particle chains. A visual representation of this process can be seen in figure 2.1.

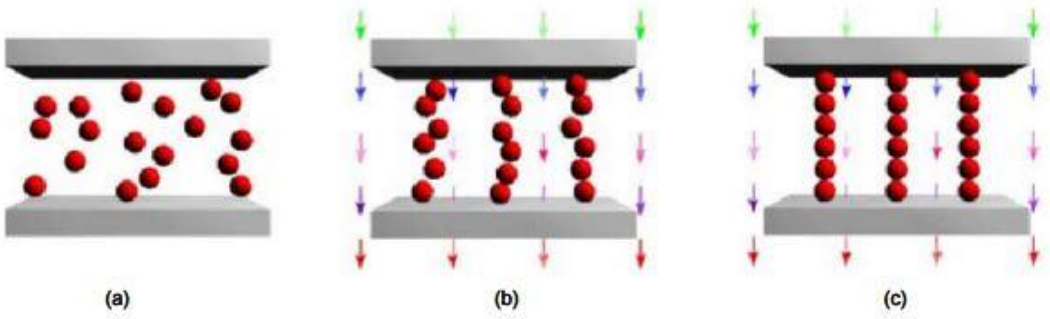

Figure 2.1: Activation of MR fluid: (a) no magnetic field applied; (b) magnetic field applied; (c) ferrous particle chains have formed (© 2005 Lord Corporation [8]. All rights reserved).

In figure 2.1 the initial condition of the MR fluid (a) is seen with the ferrous particles free flowing suspended in the fluid. When the magnetic field is applied the particles begin to align with the path of the field shown by the direction of the arrows (b). Figure 2.1(c) shows the particle chains that are formed once the particles have finished aligning with the magnetic field. These chains restrict the movement of the fluid they are suspended in, thus altering the apparent viscosity of the MR fluid substance. The time it take for this change to occur is related to the

strength of the magnetic field present and can be accomplished in a matter of milliseconds [19, 1].

2.1.2 MR Damper

A cross section of the MR dampers used in this research can be seen in Figure 2.2.

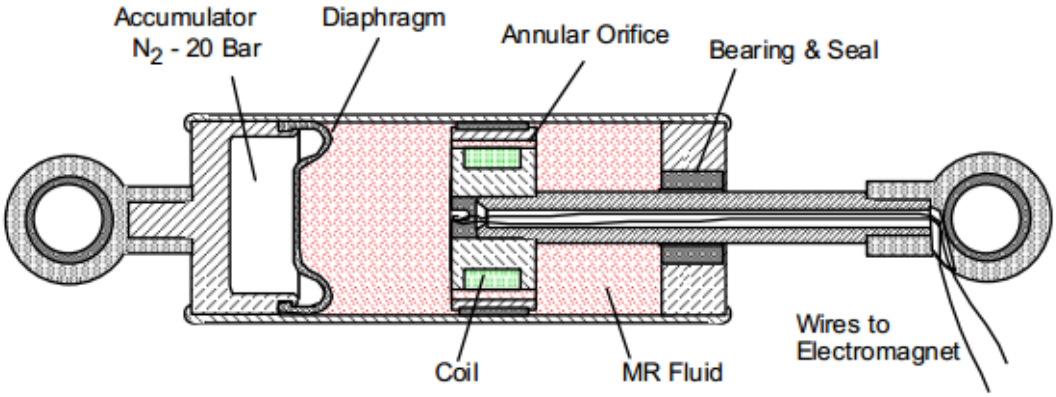

Figure 2.2: Cross section of MR damper [9].

The MR dampers consist of an internal accumulator located in the base. The main body of the damper is filled with MR fluid. A magnetic coil is placed in the valve of the damper piston, this allows the damper to alter the viscosity of the fluid passing through the valve which in turn affects the dampers stiffness. Further discussion of the MR dampers used can be found in Chapter 4.1.

2.2 Swing Arm Suspension

The Swing arm suspension system is unique to motorcycles and other two wheeled vehicles, and presents its own set of characteristics different to that seen in four wheeled vehicles or other suspension systems. Within the category of swing arm suspensions there are many

variations. Figure 2.3 shows three variations of the most common motorcycle rear swing arm suspension set ups currently used.

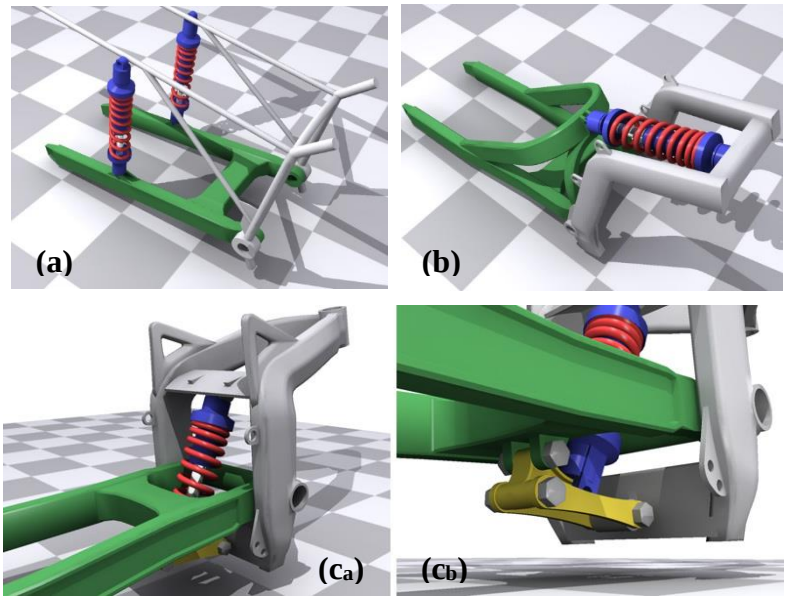

Figure 2.3: Common motorcycle rear swing arm set ups [7].

Figure 2.3(a) shows the classic interpretation of a motorcycle rear suspension system. The classic motorcycle rear suspension consists of an H shaped swing arm connected to the main frame of the vehicle at a pivot. Near the rear of the frame a damper and spring are placed on either side of the swing arm. Figure 2.3(b) shows a mono-shock older style system that was introduced into the market in the early 80's [7]. It consists of a similar H shape swing arm member with an extra horseshoe shaped member for a single shock to be mounted at the top front of the swing arm. Finally Figure 2.3(c) shows a newer style mono-shock system. This system has a single shock mounted at the front of the swing arm, similar to the old style, but reduces the amount of unsprung mass by eliminating the large horseshoe member. This is replaced by a complex linkage system under the swing arm as seen in the figure.

2.2.1 Passive suspension

Modern suspension systems are usually comprised of a hydraulic damper and a coil spring. These systems work by mitigating the amount of shock input sent into the main body of the vehicle by dissipating the input energy passing through the damper and the spring. This type of system has been used for many years, and has been enhanced and adapted to suit different applications. The limitation with this technology is that the damping device is set up with a specific purpose in mind and cannot be changed. The system may be set up with a low viscosity fluid to allow for more travel to enhance ride comfort, or the system may be set up with a stiffer suspension which would give the vehicle improved handling at the expense of ride comfort. Most automotive manufacturers find a suitable compromise between these two settings to best suit the type of vehicle and the terrain over which the vehicle is expected to travel.

2.2.2 Semi-active suspension

An active device such as a MR damper would not require such a compromise. A suspension can be soft or stiff, within the damper limits, and these characteristics can be continuously changed. Furthermore, the MR damper does not require a significant amount of energy input, and can still act as a passive damper in case of a controller failure.

There are currently three main variations of semi active control policies, all stemming from the well-known “Skyhook” policy. The other two policies are “Groundhook” and “Hybrid” control policies. The Skyhook control policy operates on the logic of the relative velocity of the damper with respect to the main body of the vehicle (sprung mass). Groundhook control policy operates on a logic that is similar to the Skyhook policy except that it is based on the relative velocity of the damper relative to the ground. A Hybrid control policy combines the logic of

Skyhook and Groundhook policies so that it can be set up as either one of the policies or a combination of both [12].

In a study performed to compare the MR fluid damper with a commercial off the shelf passive damper, the MR fluid damper reduced the maximum acceleration of mass by 13.2% for Skyhook control and 18.5% for sliding mode control [20].

Other studies have been conducted on different types of semi-active dampers. One study by Spelta, Savaresi, and Fabbri shows that semi-active damping on a motorcycle is most certainly a viable area of research. Their study consisted of implementing a single semi-active electro-hydraulic damper into the rear swing arm suspension of a motorcycle. The study focused on using a single damper stroke sensor to control a mix-1-sensor control strategy [15]. While there is no comparison between the electro-hydraulic damper and an MR damper the concepts are similar and should produce comparable results.

2.3 Chosen Techniques

For this research, a rear swing arm of a motorcycle has been selected for analysis with the application of MR dampers. Investigating a new rear suspension system for a motorcycle presents a unique opportunity to research an area that has not received much attention in the existing literature.

The majority of the research is focused on analyzing the levels of vibration mitigation that can be achieved with the MR damper at multiple excitation conditions, and at multiple configurations of the damper. Many experiments on MR damper vibration mitigation focus on a single input transferring through a single damping system. This type of system is referred to as a “quarter car” system since it represents one of the four wheels on a car. The type of motorcycle

rear swing arm suspension investigated in this research offers a distinctive difference from the quarter car model. A single input point is representative of the road profile at the rear tire, but the load is transferred through two separate damping devices. This leads to a distinctive model of the suspension set up and could lead to interesting results from this research.

2.4 Conclusions

As discussed in this chapter, MR fluid is an exciting technology that has many promising applications. One of the most common applications of MR fluid is in dampers, creating a system that can change the stiffness level of a damper at a moment's notice.

The purpose of this research is to explore the possibilities of using MR damping devices in motorcycle applications. For the purposes of this research it has been decided to analyze a rear swing arm suspension system. Using a dual damper system that is approximated as a half-car model, pre-established control policies will be used to analyze vibration mitigation. The system will be excited by using a shaker table and the payload will be attached to the top portion of the damper and the swing arm set up. Data will be collected using several accelerometers placed in key areas on the test set up as well as the payload.

CHAPTER 3: MATHEMATICAL MODELING

This chapter presents the mathematical models that have been developed during this study. The main purpose of these models is to comprehend the influence of semi-active damping on the dynamics of the system. Some of the computational tools that were used during this study are also discussed in this chapter.

3.1 Transmissibility

Transmissibility is a term used in this study to assess the damping characteristics of the system. Specifically, transmissibility is used to identify the response amplitude of the payload. "*Transmissibility is the nondimensional ratio of the response amplitude of a system in steady-state forced vibration to the excitation amplitude. The ratio may be one of forces, displacements, velocities, or accelerations.*" [6]

The transmissibility of a system consists of three main factors, the displacement transmissibility (T_d), the acceleration transmissibility (T_a), and the force transmissibility (T_f). Figure 3.1 shows a single degree-of-freedom (DOF) spring-mass-damper system with a base excitation.

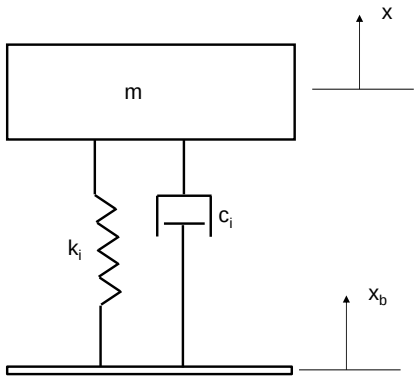

Figure 3.1: Single DOF model with base excitation.

The governing equation of motion (EOM) for the single degree-of-freedom spring-mass-damper system shown in Figure 3.1 is as follows:

$$m\ddot{x} + c_i(\dot{x} - \dot{x}_b) + k_i(x - x_b) = f \qquad \text{(Eq. 3.1)}$$

In Equation 3.1, k_i and c_i are the stiffness and damping constants of the MR damper, x and x_b are the displacements of the mass and the base respectively, and f is the excitation force applied to the base. The subscript 'i' is used to indicate the dependence of the stiffness and damping of the MR damper on the current input to the electromagnet. Displacement transmissibility (T_d) and acceleration transmissibility (T_a) are expressed as the ratio of the mass displacement and the base displacement, and the ratio between the mass acceleration and the base acceleration:

$$T_d = \frac{x}{x_b} = T_a = \frac{\ddot{x}}{\ddot{x}_b} = \left[\frac{1+(2\zeta_i r_i)^2}{\left(1-r_i^2\right)^2+(2\zeta_i r_i)^2}\right]^{1/2} \qquad \text{(Eq. 3.2)}$$

In Equation 3.2, ζ_i is the damping ratio and r_i is the frequency ratio between the base excitation frequency and the natural frequency of the system (ω_n). Force Transmissibility can in turn be calculated from the displacement or acceleration transmissibility as:

$$T_f = r_i^2 T_d = r_i^2 T_a \qquad \text{(Eq. 3.3)}$$

In systems with passive damping, transmissibility is determined from an assessment of the needs of a system. Figure 3.2 shows how changing the damping ratio (ζ) changes the displacement transmissibility in a traditional passive system.

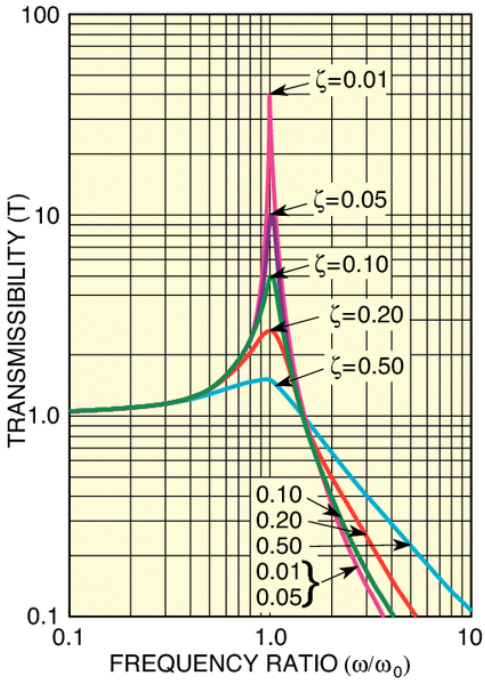

Figure 3.2: Transmissibility of a damped oscillator system with various values of the damping coefficient (ζ) [11].

MR dampers have the unique ability to alter their transmissibility behavior by changing the stiffness and damping properties of the damper. In this research, the damper characteristics have been found at varying current inputs to the electromagnet of the damper. A Universal Testing Machine has been used to test the MR dampers used for this study. More details about this testing and the test equipment are provided in Chapter 4. Table 3.1 shows the calculated stiffness and damping constants calculated from the test results at different current levels.

Table 3.1: MR damper characteristics.

Current (A)	k_i (N/m)	c_i (N-s/m)	ζ_i (m = 11.5 kg)	ζ_i (m = 14.9 kg)
0	100	2.5	0.037	0.032
0.5	150	20	0.240	0.211
1	150	30	0.361	0.317
1.5	150	37.5	0.451	0.396

Figures 3.3 and 3.4 show the displacement and force transmissibility plots for the MR dampers used in this study. These plots are based on the data in Table 3.1, using a single DOF model shown in Figure 3.1.

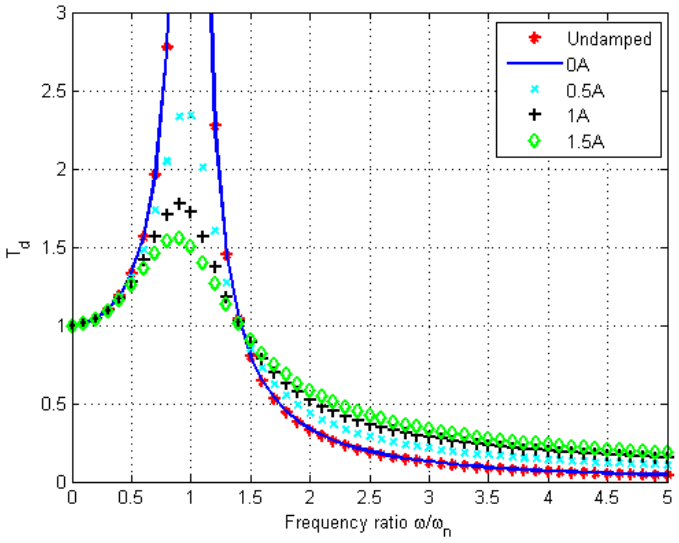

Figure 3.3: Displacement transmissibility plot.

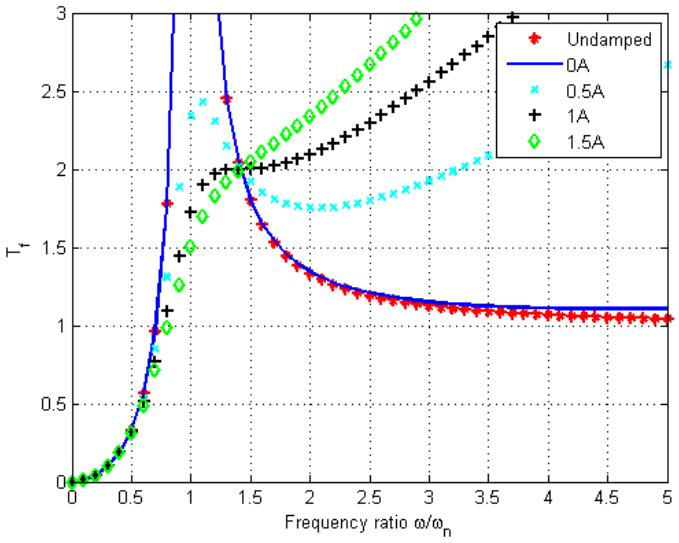

Figure 3.4: Force transmissibility plot.

The transmissibility behavior of both the passive damping system and the MR damping system can be seen to be very similar. Both systems display an unavoidable amplification over a range of frequencies. Traditional methods of eliminating this amplification include ensuring that normal operating conditions remain outside of the frequency range or increasing the damping ratio to mitigate amplification. Increasing the damping ratio, however, comes with the cost of increasing the displacement and force transmissibility at relatively higher frequencies.

Due to the nature of MR dampers and their ability to change the damping ratio by simply altering the current input, the problem of being forced to select one specific transmissibility curve to fit a system is significantly resolved. This technology allows an ability to have a high damping ratio over amplification frequencies, and then having a reduced damping ratio over higher frequencies. This ensures an efficient transmissibility curve over the entire relevant frequency range. Figures 3.5 and 3.6 show two such examples of the influence of altering the damping ratio to yield a suitable transmissibility plot.

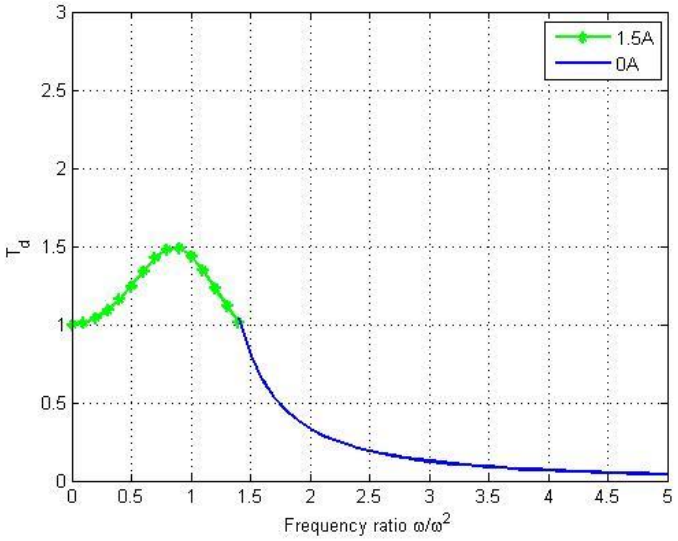

Figure 3.5: Modified displacement transmissibility plot.

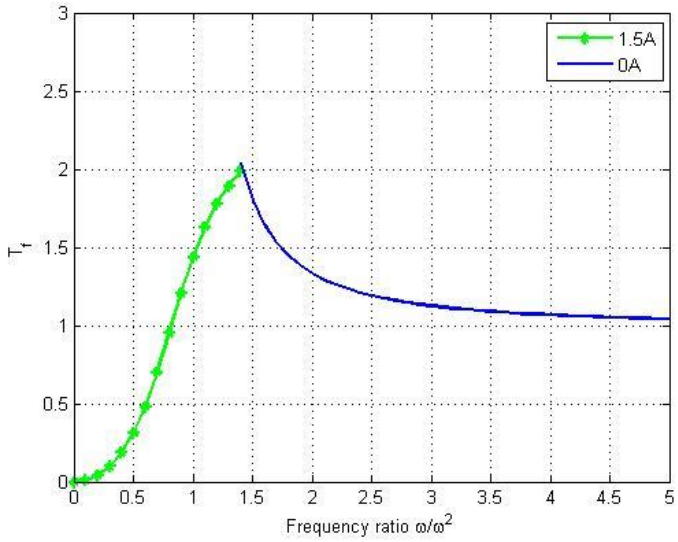

Figure 3.6: Modified force transmissibility plot.

3.2 Frequency Response

One of the most common means of interpreting data procured from vibration testing is the use of frequency response. During vibration testing, data is collected in terms of time history of acceleration. This data provides the acceleration response at each specific point at different instances in time. In order to interpret the data, the time history is transformed into the frequency domain. By transforming the data into frequency domain, the acceleration magnitude can be observed for a range of frequencies. This response clearly demonstrates the range of frequencies over which the system exhibits amplification and mitigation of vibration.

It is a common practice to filter the data before transforming into frequency domain. Filtering the time history removes noise or external vibrational inputs that are inevitable during testing and data acquisition and prevents aliasing. For this study, a fourth order Butterworth filter has been used. This filter is seen to sufficiently capture the relevant data without any significant noise effects. Most of the testing has been performed by using a frequency sweep of 5Hz to

100Hz as an excitation input to the system. A high pass filter set with a cutoff frequency at 1Hz and a low pass filter with a cutoff frequency at 105Hz ensures that any noise outside the excitation range is excluded. Equation 3.4 shows the generalized form of a Butterworth filter:

$$H_{(j\omega)} = \frac{1}{\sqrt{1+\varepsilon^2(\frac{\omega}{\omega_P})^{2n}}} \qquad \text{(Eq. 3.4)}$$

In Equation 3.4, ω is equal to $2\pi f$ and ε is the maximum pass band gain [16].

Once the data is filtered, it is transformed into the frequency domain for further analysis. A typical time domain signal can be represented in the frequency domain by using the Fourier Transform. The Fourier Transform decomposes a time ordered signal into the frequencies present in that signal. The Continuous time Fourier series (CTFS) representation for a periodic excitation can be written as follows:

$$x(t) = \sum_{m=-\infty}^{\infty} c_m e^{jm\omega_0 t}; \quad where \quad \omega_0 = \frac{2\pi}{P} \qquad \text{(Eq. 3.5)}$$

In Equation 3.5, c_m are the Fourier series coefficients and are computed as:

$$c_m = \frac{1}{P}\int_{-P/2}^{P/2} x(t)e^{-jm\omega_0 t}\,dt \qquad \text{(Eq. 3.6)}$$

In Equation 3.6, ω_0 is the fundamental frequency and P is the fundamental period of the function $x(t)$. The Discrete time Fourier series (DTFS) representation of the corresponding discretized function is as follows:

$$x[n] = x(nT) = \sum_{m=<N>} c_{md}\, e^{jm\omega_0 nT} \qquad \text{(Eq. 3.7)}$$

Where $\omega_0 = \frac{2\pi}{NT}$. In Equation 3.7 c_{md} are the Fourier series coefficients and are computed as

$$c_{md} = \frac{1}{N}\sum_{n=0}^{N-1} x[n]\, e^{-jm\omega_0 nT} \qquad \text{(Eq. 3.8)}$$

In Equation 3.8, ω_0 is the fundamental frequency and T is the sampling period. For an approximately band-limited function, $x(t)$, and correctly chosen sampling period, T, the CTFS coefficients can be computed from the corresponding DTFS coefficients. DTFS coefficients can, in turn, be computed by using the Fast Fourier Transform (FFT).

$$c_{md} = \frac{X[m]}{N} \qquad \text{(Eq. 3.9)}$$

In Equation 3.9 $X[m]$ is the FFT of $x[n]$ and N is the number of terms of $x[n]$ used in computing the FFT.

The Continuous time Fourier transform (CTFT) of a function is defined as follows:

$$X(\omega) = \int_{-\infty}^{\infty} x(t) e^{-j\omega t} dt \qquad \text{(Eq. 3.10)}$$

In Equation 3.10, $X(\omega)$ is called as the spectrum or the frequency response of $x(t)$ and can be defined for periodic as well as non-periodic functions.

The Discrete time Fourier transform (DTFT) for the corresponding discretized function is expressed as follows:

$$X_d(\omega) = \sum_{n=-\infty}^{\infty} x(nT) e^{-j\omega nT} \qquad \text{(Eq. 3.11)}$$

If the frequency aliasing due to time sampling is negligible, i.e. for a sufficiently small T, CTFT and DTFT are related as follows [2]:

$$|X(\omega)| \approx T|X_d(\omega)| \qquad \text{(Eq. 3.12)}$$

The spectrum of $x(t)$, $X(\omega)$, can be computed from its sampled sequence $x[n]$ even if $x(t)$ is not exactly band-limited. $X_d(\omega)$ can be computed using the FFT and the magnitude spectrum of $X(\omega)$ can be obtained using Equation 3.12.

The Fast Fourier Transform proves to be very useful in the analysis of both periodic and non-periodic profiles with a known function. Since *x(t)* is time-limited for most of the excitations used in this study, no truncation effects are observed. Effects of frequency aliasing are avoided by iteratively reducing the sampling time till aliasing is minimized. For all the excitation inputs used in this study, the final sampling period is obtained by iteratively reducing *T* and comparing the maximum magnitude of the spectrum with that of the previous spectrum.

For this study, the frequency response of the data is found by implementing a Fast Fourier Transform on the data set collected in the form of time history. The use of the FFT is found to be convenient. The FFT algorithm in MATLAB has been used for computing all the frequency responses in this study. Equation 3.13 summarizes the algorithm used in MATLAB [10] for calculating FFT.

$$X(k) = \sum_{j=1}^{N} x(j)\omega_N^{(j-1)(k-1)} \qquad \text{(Eq. 3.13)}$$

3.3 Swing Arm Model

Since the main objective of this study is to investigate the application of MR dampers in a swing arm suspension system, a preliminary lumped mass model has been developed as a reference. The swing arm structure as well as the suspension system are briefly described in this section.

As with any mechanical system that has been in use for a long period of time, many advanced, modified, and alternate swing arm suspension designs exist. The most simple and traditional swing arm system is the twin-shock regular swing arm fork. Figure 3.7 depicts one such system.

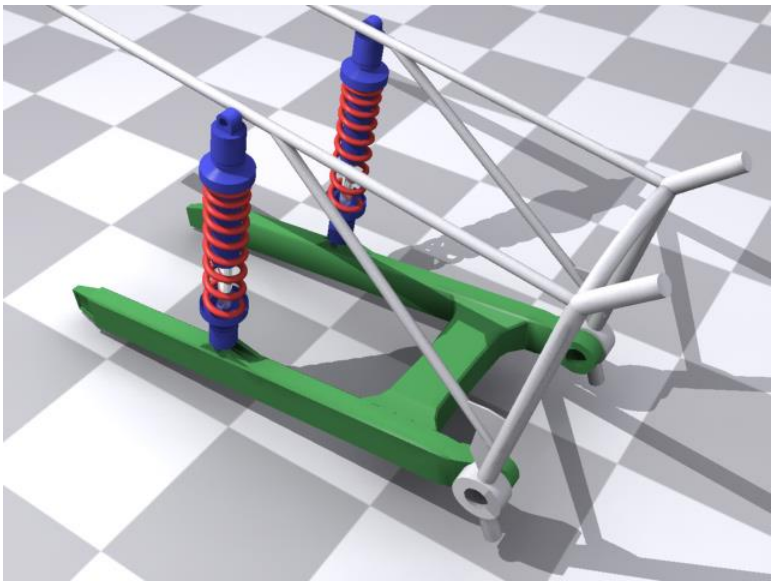

Figure 3.7: Twin-shock regular swing arm fork [7].

This style of suspension consists of two beams connected in the middle to form an H-shape fork arm. The front of the arm is attached to a pivot connected to the main frame of a motorcycle. Two shock absorbers are mounted at the bottom near the rear axle and attach to the frame along the seat rail. Other swing arm suspension systems include top and bottom mounted mono shock setups, double and single swing arm forks, and even a monolever which consists of a larger single swing arm that houses a drive shaft [7, 3].

The classic twin-shock regular swing arm fork has been used as a reference for this study. As a result, the test fixture represents the geometry of a typical dual-shock system. This style has been chosen because it presents the best and simplest conditions for testing the feasibility of using MR dampers in a swing arm configuration.

To predict the behavior of the classic twin-shock regular swing arm fork suspension system, a mathematical model representation has been developed. Three possible models for representing the system in different aspects about the system are shown below.

Model 1 shown in Figure 3.8 is the simplest representation, showing a rear view depiction of the spring-mass-damper system.

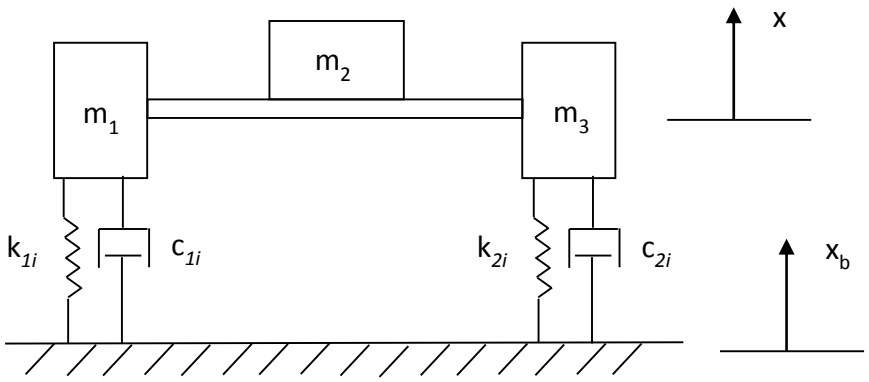

Figure 3.8: Model 1.

In Model 1, m_1 and m_3 are the secondary masses, m_2 is the main payload mass, k_{ni} is the spring stiffness of the damper, c_{ni} is the damping coefficient, x is the measured output, and x_b is the base input excitation (displacement). Model 1 represents two spring-dampers connected directly to the input excitation. Two masses are placed directly above the dampers and a third payload mass is attached between the two dampers. The payload and both secondary masses are rigidly attached to each other and the system is assumed to be symmetrical about the center axis. The in-plane dynamics of Model 1 can be represented by the following equations of motion:

$$(m_1 + m_2 + m_3)\ddot{x} + (c_{1i} + c_{2i})(\dot{x} - \dot{x}_b) + (k_{1i} + k_{2i})(x - x_b) = 0 \qquad \text{(Eq. 3.14)}$$

$$\frac{x}{x_b} = \frac{\ddot{x}}{\ddot{x}_b} = T = \left[\frac{1+(2\zeta_i r_i)^2}{\left(1-r_i^2\right)^2+(2\zeta_i r_i)^2}\right]^{1/2} \qquad \text{(Eq. 3.15)}$$

$$\zeta_i = \frac{c_{1i}+c_{2i}}{2\sqrt{(m_1+m_2+m_3)(k_{1i}+k_{2i})}} \qquad \text{(Eq. 3.16)}$$

$$r_i = \frac{\omega}{\omega_{ni}} \qquad \text{(Eq. 3.17)}$$

$$\omega_{ni} = \sqrt{\frac{(k_{1i}+k_{2i})}{(m_1+m_2+m_3)}} \qquad \text{(Eq. 3.18)}$$

It may be noted that the symbols in Equation 3.14 to Equation 3.18 are identical to the terminology used in Sections 3.1 and 3.2.

Model 2 represents a system that is similar to Model 1, assuming the system is symmetrical with identical masses on either side, and the payload is at the center. However, Model 2 introduces the tire into the system as a separate attachment with unsprung masses. Model 2 is shown in Figure 3.9.

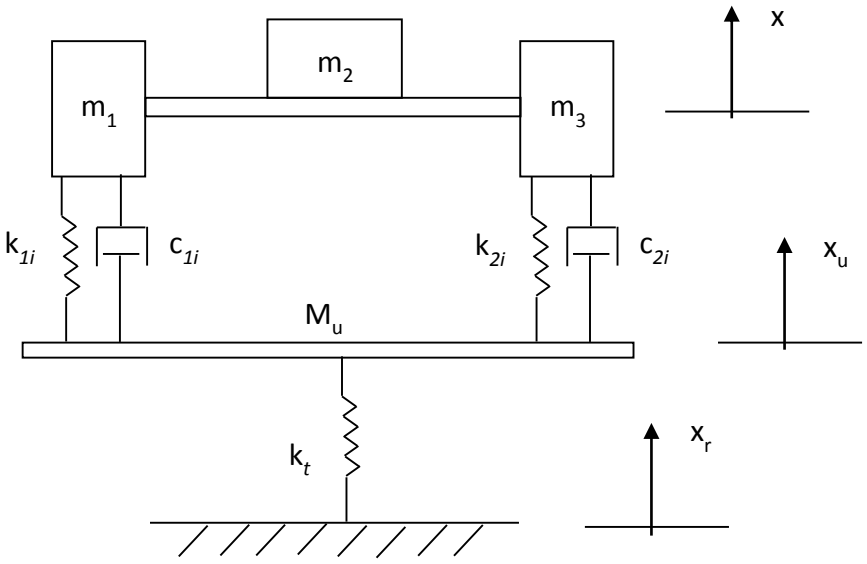

Figure 3.9: Model 2.

In Model 2, m_u is the unsprung mass, x_u is the displacement of the unsprung mass, k_t is the tire stiffness, and x_r is the road input excitation (displacement). The in-plane dynamics of Model 2 can be expressed by the following equations of motion:

$$(m_1 + m_2 + m_3)\ddot{x} = k_{1i}(x_u - x) + k_{2i}(x_u - x) + c_{1i}(\dot{x}_u - \dot{x}) + c_{2i}(\dot{x}_u - \dot{x}) \quad \text{(Eq. 3.19)}$$

$$m_u\ddot{x}_u = k_t(x_r - x_u) - k_{1i}(x_u - x) - k_{2i}(x_u - x) - c_{1i}(\dot{x}_u - \dot{x}) - c_{2i}(\dot{x}_u - \dot{x}) \quad \text{(Eq. 3.20)}$$

These equations of motion are coupled together. The representation of the unsprung mass in the equations of motion captures the dynamics of the masses attached to the wheel.

Model 3 is the final model presented in this section. This model is similar to the other two models but the main payload mass is off-set, so the center of gravity is not at the geometrical center of the system. Model 3 is shown in Figure 3.10.

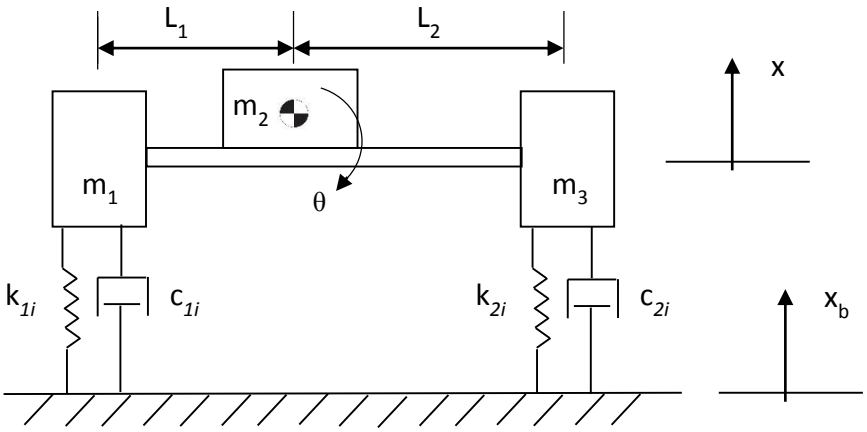

Figure 3.10: Model 3.

The in-plane dynamics of Model 3 can be expressed by the following equations of motion:

$$(m_1 + m_2 + m_3)\ddot{x} = k_{1i}(x + L_1\theta) + k_{2i}(x - L_2\theta) + c_{1i}\left(\dot{x} + L_1\dot{\theta}\right) + c_{2i}\left(\dot{x} - L_2\dot{\theta}\right) \quad \text{(Eq. 3.21)}$$

$$J\ddot{\theta} = k_{1i}(x + L_1\theta)L_1 - k_{2i}(x - L_2\theta)L_2 + c_{1i}\left(\dot{x} + L_1\dot{\theta}\right)L_1 - c_{2i}\left(\dot{x} - L_2\dot{\theta}\right)L_2 \quad \text{(Eq. 3.22)}$$

In Model 3, *J* is the mass moment of inertia about the centroidal axis. In this case, the translational motion is coupled to the rotational motion. It may be noted that all other variables are identical to the previous two models.

3.4 Vibration Control

An interesting aspect of MR damping is that the damping can be controlled actively, simply by changing the input current to the electromagnet of the damper. This function of MR dampers leads to a large area of research for MR dampers as well as the control systems

associated with implementing active control. A preliminary investigation into a vibration control system has been conducted, and a control algorithm has been simulated. This simulation is briefly discussed in this section.

There are three main variations of semi-active control policies, all stemming from the foundation "Skyhook" algorithm. The other two algorithms are called as "Groundhook" and "Hybrid" control. Skyhook control operates on the logic of the relative velocity of the damper with respect to the main body of the vehicle (sprung mass). Groundhook control operates on a logic that is similar to the Skyhook policy except that it is based on the relative velocity of the damper relative to the ground. Hybrid control combines the logic of Skyhook and Groundhook algorithms so that it can be set up as either one of the two algorithms or as a combination of both [12].

The development of a vibration control algorithm using MR dampers is a non-trivial problem. It may be easy to visualize the damping needed by a system at a specific instance of time. However, the required level of damping cannot be directly delivered by the MR damper. An input current to the electromagnet can be used as the control variable, but the relationship between the input current and damping is complex. The damping level is dependent upon many factors in addition to the input current to the electromagnet, such as displacement, velocity and acceleration, temperature, etc. Out of all these factors, the only factor that can be directly controlled is the input current. To create a vibration control algorithm, the required damping level, the present damping level, and the current level are all needed to exhibit damping control in real time with a feedback loop.

The control loop has been implemented in a simulation using a Simulink® model by using the Skyhook control algorithm [17], as seen in Figure 3.11.

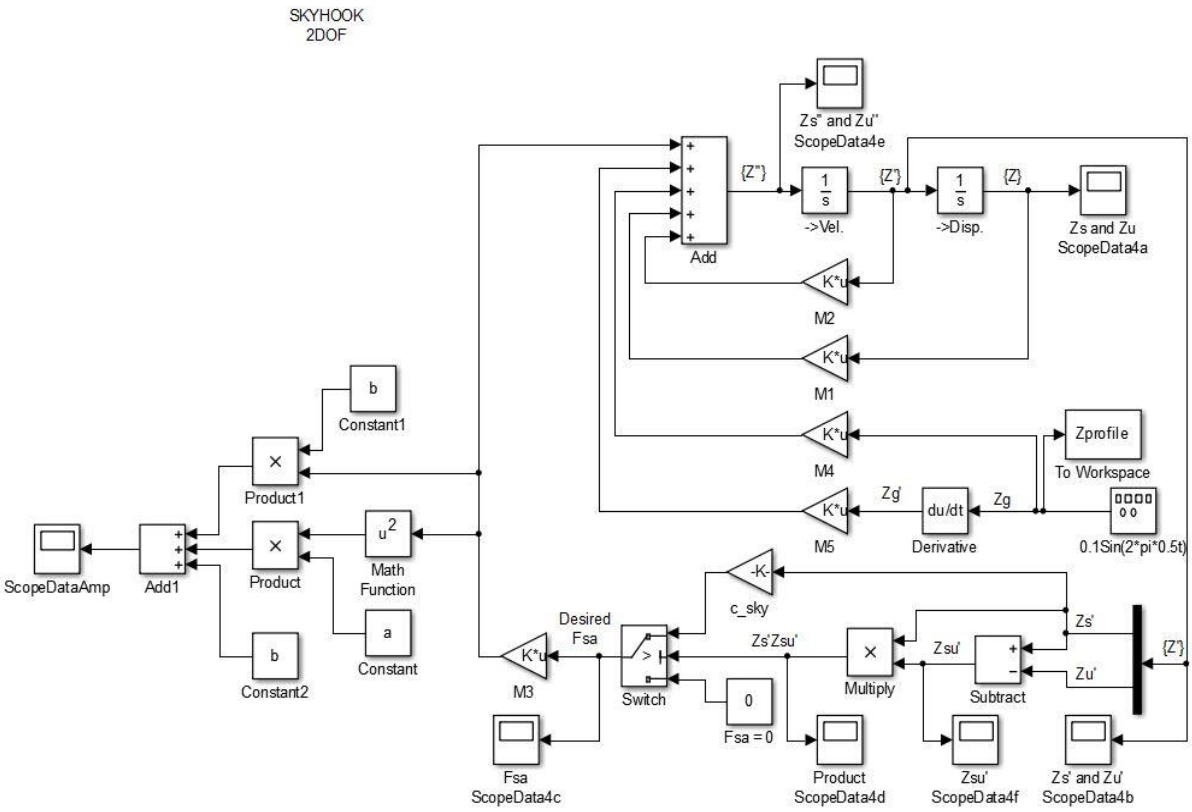

Figure 3.11: Simulink® Skyhook control algorithm.

The Simulink model seen in Figure 3.11 uses a sine wave to create an acceleration input signal. This signal is used to calculate the velocity and displacement of the input. The velocity signal is then used to control the Skyhook algorithm. The present velocity is compared to the previously recorded velocity. If there is a difference between the present velocity and the previous velocity, a semi-active damping response force is calculated to maximize the damping efficiency. The damping response force is calculated by multiplying the present velocity by a gain factor as seen in Equation 3.23.

$$C_{sky} = 2\zeta\sqrt{k_s M_s} \qquad \text{(Eq. 3.23)}$$

In Equation 3.23, C_{sky} is the calculated damping constant, ζ is the damping ratio, k_s is the stiffness, and M_s is the sprung mass. If there is no change in the velocity, or if the change is negative, the response force is left at zero. The current acceleration, velocity, position, and response force are fed in a loop to determine the next state of the system.

Before the control algorithm can be simulated, it must be adapted to the specific application involving the MR dampers. In the case of this research, two MR dampers manufactured by LORD Corporation (Part No: RD-8041-1) are used for damping. Compression testing on the dampers was performed to gain an understanding about the performance of MR dampers at different current inputs under various conditions. Figure 3.12 shows the results from one of these compression tests where the damper was exposed to a constant velocity of 10mm/min.

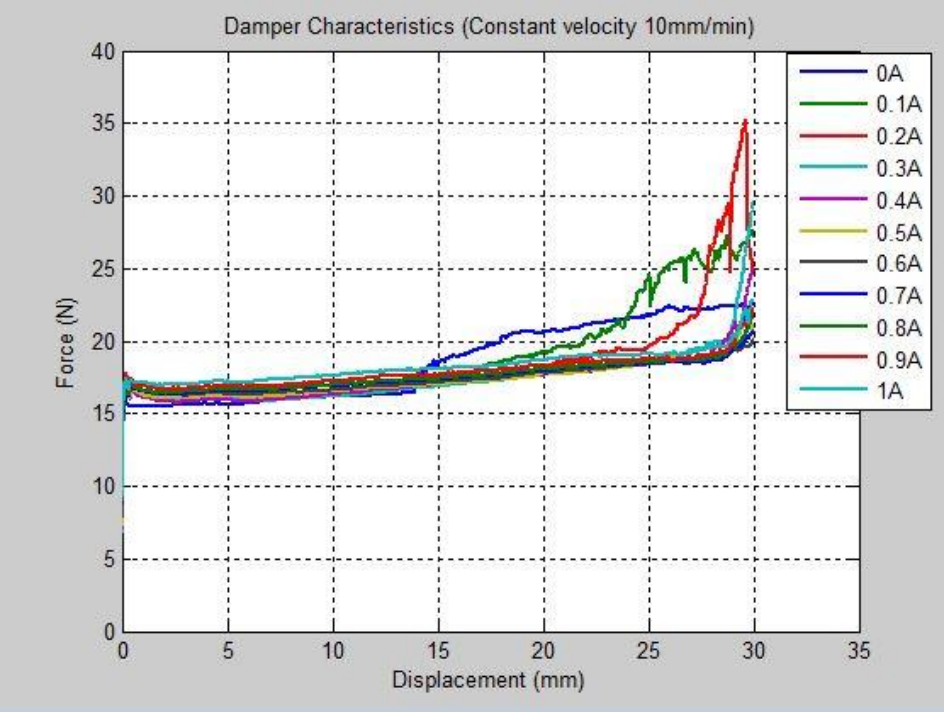

Figure 3.12: Constant velocity compression test results.

This testing provided data that is used to develop a polynomial equation to relate the required damping force to the actual current needed to produce that damping force. Only the linear section of data from 5mm to 10mm displacement has been used to develop the control equation. The data is normalized about the value of mean force. Equation 3.24 has been derived from the data using a second order polynomial equation as shown below:

$$I = -0.31(f)^2 + 0.75(f) + 0.57 \qquad \text{(Eq. 3.24)}$$

In Equation 3.24, *f* is the required damping force and *I* is the input current to the electromagnet. Once the equation to calculate the control current is identified, the control algorithm is implemented in the Simulink® model.

The simulation was run for 60 seconds. Figure 3.13 shows the force response required from the MR damper while Figure 3.14 shows the converted force response to the input current required for control.

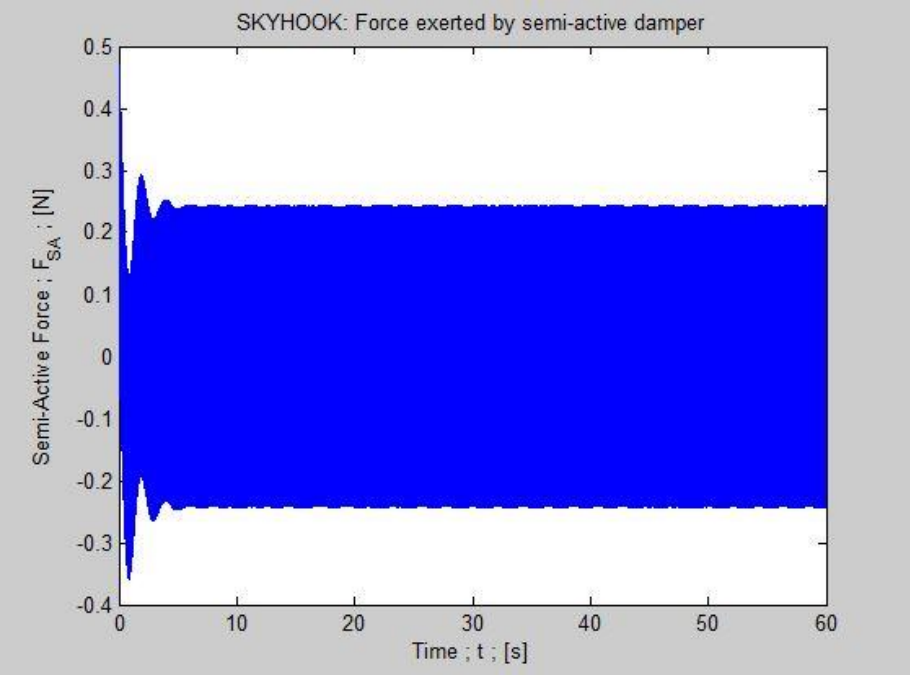

Figure 3.13: Required damping force.

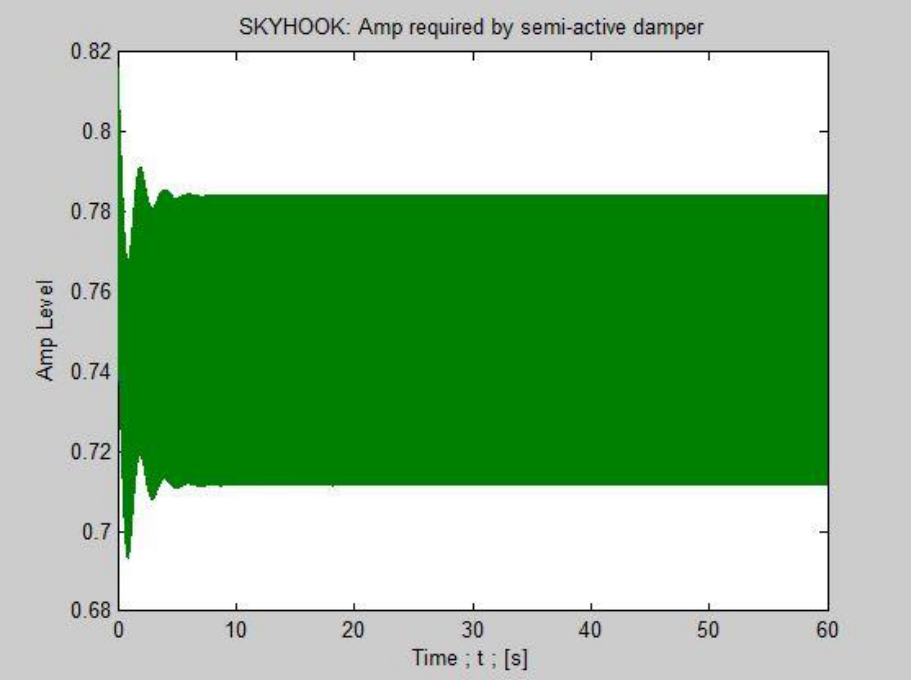

Figure 3.14: Calculated current input.

These results show that the simulation is consistent with the expected relationship with the damping force and the control current. However, this simulation provides only a starting point for the implementation of a full control policy for this system. This simulation only applies to a small range of displacement of the dampers at a constant velocity input. To develop a full control policy for this system, more research must be done to comprehend the influence of other variables affecting control characteristics and damping force.

3.5 Conclusions

This chapter presented the mathematical models that have been developed during this study to comprehend the performance of MR dampers in a swing arm suspension. Also included in this chapter is the necessary information on the behavior of a spring-mass-damper system and possible models that can be used to comprehend the in-plane characteristics of the swing arm

suspension system. The characteristics of transmissibility and the specific parameters that have been identified for the dampers used for testing have been presented.

Frequency response is used to interpret the data collected in time domain data by transforming the data into the frequency domain. The process of filtering the data and transforming the data into frequency domain has also been briefly discussed in this chapter. Three possible mathematical models that can be used for representing the swing arm suspension are presented, and a simulation for a Skyhook control algorithm that could be used in semi-active vibration control for the system is briefly discussed.

CHAPTER 4: EXPERIMENTAL RESULTS

This chapter provides an overview of the equipment, machinery, and test fixtures used during this research. Line diagrams are also presented to demonstrate the connections between the inputs, the measured signals, and the data collection unit. Data has been post-processed and the damping results are presented along with necessary discussion.

4.1 Experimental Setup

The test setup includes an Agilent 33220A waveform generator, shown in Figure 4.1, used for creating a sinusoidal function or a sweep of sinusoidal functions. Various frequencies and amplitudes can be generated, depending on the required test parameters. The output of the waveform generator is transmitted to the controller that amplifies the signal and controls the excitation input to the shaker table.

Figure 4.1: Agilent 33220A waveform generator.

For this study, a fixture was designed and fabricated in order to represent the rear swing arm suspension system of a motorcycle with a dual shock. The fixture was designed so as to simulate the shape, geometry, and degrees of freedom associated with the suspension system. The main structure was made of 80/20® Aluminum. This material was chosen due to ease of manufacturing and assembly. Furthermore, this material significantly mitigated the overall payload mass that the shaker table needs to support. The front end of the fixture was attached to a grounded fixture that was isolated from the input vibration, as shown in Figure 4.2.

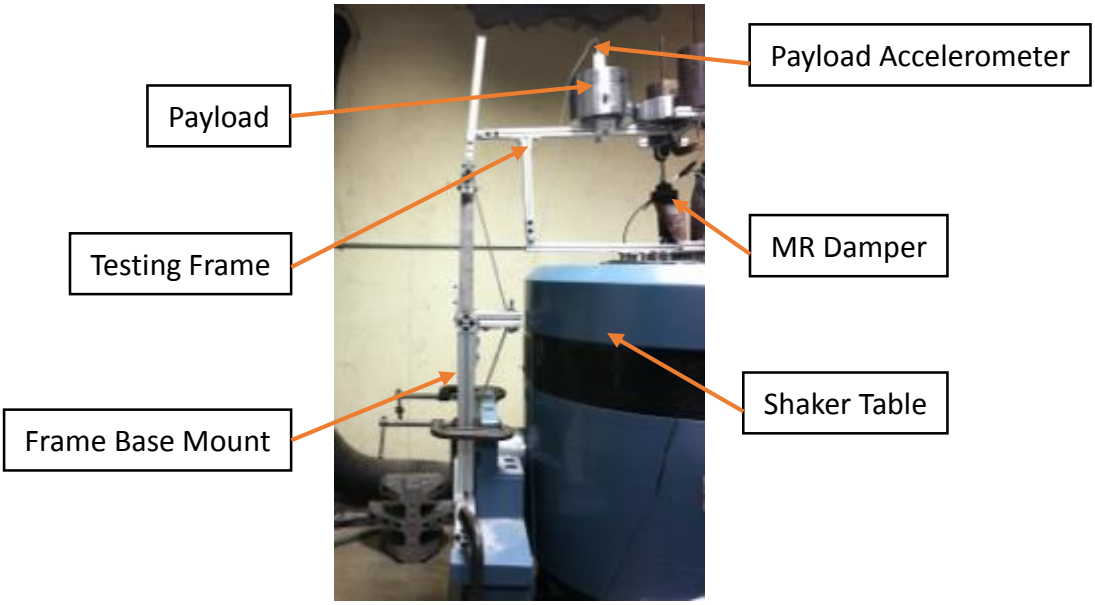

Figure 4.2: Shaker table – test fixture.

As seen in Figure 4.2, the front section of the frame is securely clamped to the base of the shaker table. This support structure is made of 80/20® Aluminum and reinforced with steel supports to enhance structural rigidity. At the top of the support structure, there are two pivoting hinges that allow the whole swing arm assembly to travel horizontally and rotate about the support structure as it travels vertically during testing. Figure 4.3 shows a close view of the complete test fixture mounted on the shaker table.

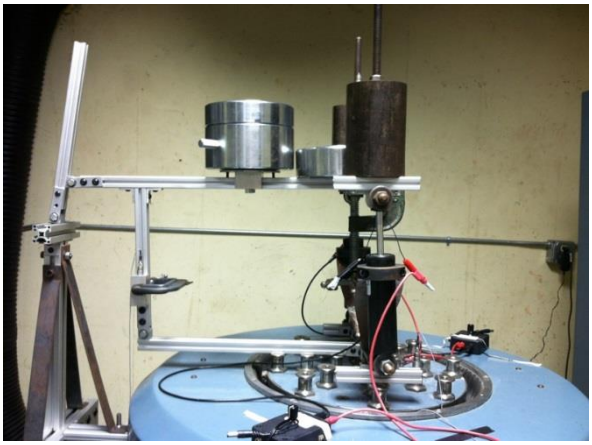

Figure 4.3: Test fixture – close up.

The swing arm test frame is made from two T-sections rather than creating a frame with two arms that may closely resemble a commercial product. This is done to reduce the overall mass of the frame. The bottom “axle” portion of the swing arm frame is connected to the shaker table through a bolted joint. The top portion of the frame is allowed to pivot at the start of the swingarm. The damper used in this test setup is shown in Figure 4.4. Two such dampers are used in the test setup.

Figure 4.4: LORD MR damper and control module.

A set of two MR dampers manufactured by LORD Corporation (Part No: RD-8041-1) are used in the testing fixture. Figure 4.5 shows one of these dampers along with the controller module that is used to control the input current to the damper.

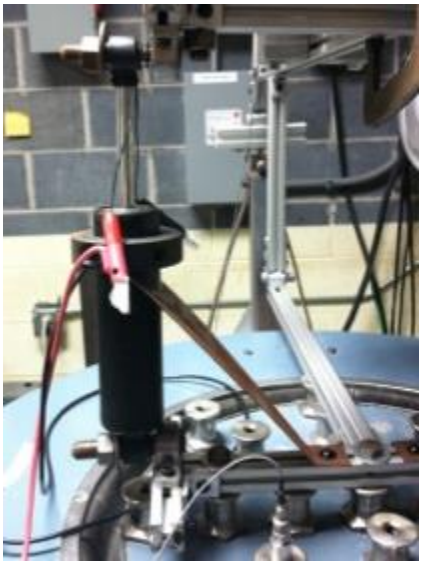

Figure 4.5: Assembled damper.

Figure 4.5 shows the dampers bolted to the frame with a 0.5” threaded shaft that is attached to self-lubricating aluminum-mounted Bronze bearings (Manufacturer: McMaster-Carr, Part No: 5912K4). The assembly is supported laterally by using steel flanges that are attached to a collar around the lower portion of the dampers. Figure 4.6 shows an exploded view of the CAD model for the suspension assembly that has been designed and manufactured for this study.

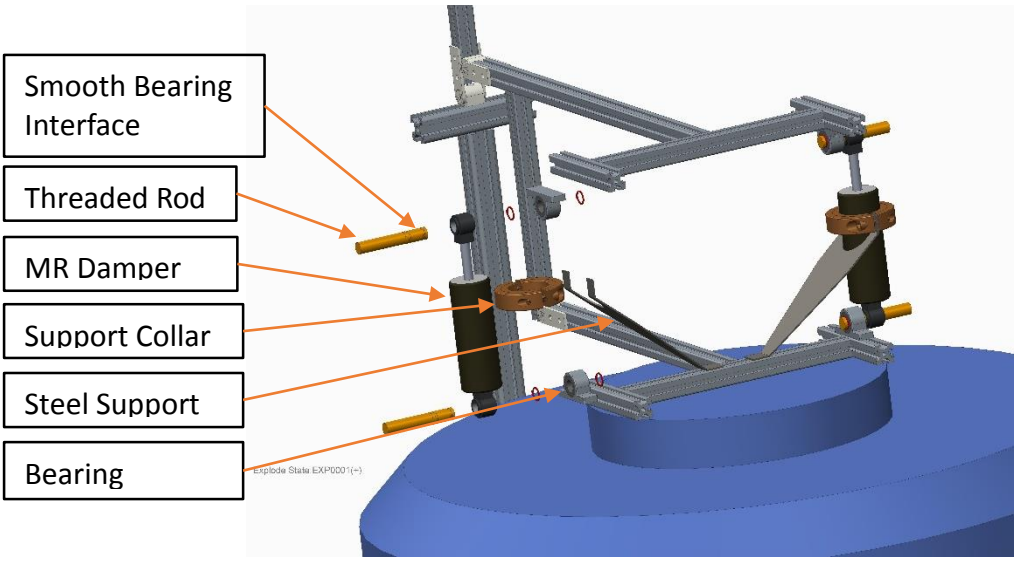

Figure 4.6: CAD model exploded assembly.

Several lumped masses were used iteratively to represent the payload in the testing fixture. The main payload mass of 14.9kg is located approximately at the rider seating position in a motorcycle, with respect to the pivot point of the swing arm. This payload mass is directly bolted to the frame by using an aluminum adapter plate. During preliminary testing it was found that the payload mass was not adequate to pre-compress the dampers during testing. As a result, two additional masses were included in the test setup, two masses of 6.5kg each. These masses were positioned right above the dampers and directly connected to the frame to provide a preload for compressing the dampers before starting any testing. After additional testing, it was determined that a third mass was necessary to prevent the dampers from reaching a maximum

stroke during testing. A mass of 6.6kg was added between the three existing masses and clamped in place, as shown in Figure 4.7.

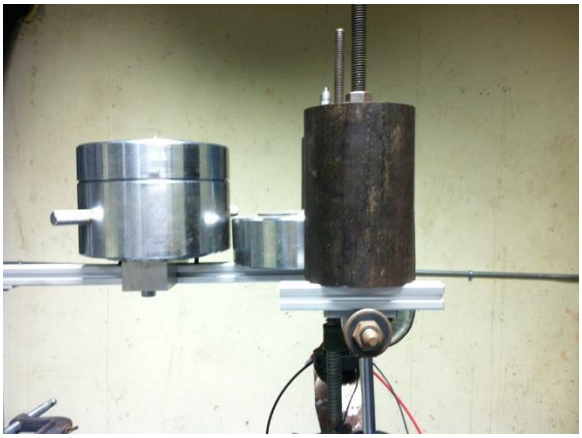

Figure 4.7: Payloads on test setup.

The tensile testing machine (Instron® 5967), shown in Figure 4.8, was used for initial compression testing of the MR damper in order to determine the stiffness and damping characteristics of the damper at multiple current inputs and multiple frequencies. Several tests were run to analyze the load-displacement characteristics at different currents. This data was used to determine the capabilities of the damper, and subsequently used to compare results taken from vibration testing. Figure 4.8 shows the tensile tester while loading one of the MR dampers during an initial trial performed for this study.

Figure 4.8: Tensile test for damper.

Accelerometers were used to quantify the level of vibration mitigation provided by the damping system at multiple levels and settings, or at multiple levels of excitation. A pair of DYTRAN 3019A accelerometers have been used for testing. One such accelerometer is shown in Figure 4.9.

Figure 4.9: DYTRAN 3019A accelerometer.

During the first round of testing, one accelerometer was positioned on top of the main payload mass as shown in Figure 4.10, and a second accelerometer was positioned directly on top of the top surface of the shaker table top. This setup was adequate to directly measure the acceleration input from the shaker table and the resulting acceleration observed by the payload.

For the second round of testing, the main payload accelerometer was moved to the top of the mass located above the damper, and a third accelerometer was added. The third accelerometer was positioned approximately at a location where the rider's foot peg is located on a motorcycle. All locations of the accelerometers are shown in Figure 4.11.

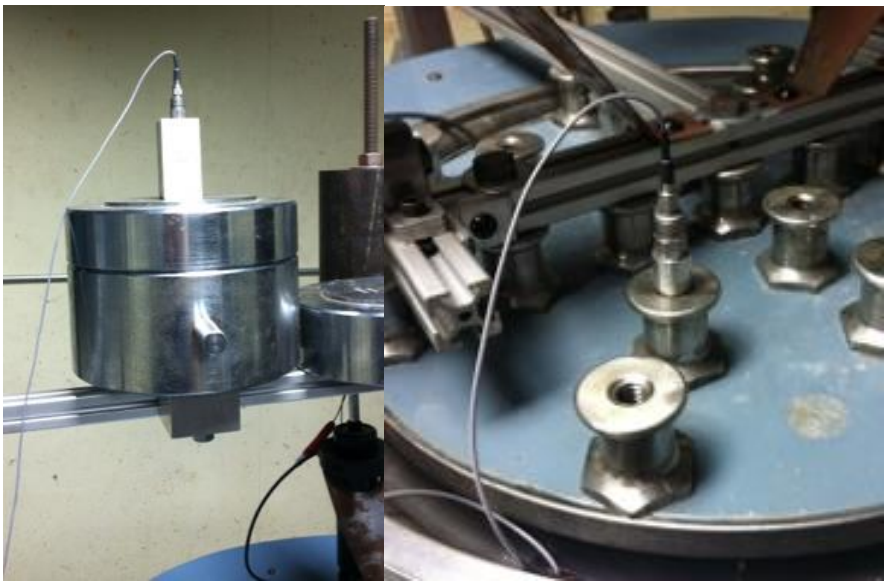

Figure 4.10: Accelerometer setup – first round testing.

Figure 4.11 Accelerometer setup – second round testing.

A National Instruments™ (NI) data acquisition unit (c-DAQ-9172) along with multiple accelerometer modules (NI9234) have been used for data acquisition. Figure 4.12 shows the accelerometer module and Figure 4.13 shows the c-DAQ system.

Figure 4.12: NI9234 accelerometer module.

Figure 4.13: National Instruments^{TM} c-DAQ-9172.

A laptop is required to connect to the c-DAQ system in order to perform data collection. Data from all test iterations has been collected through LabView and post-processed in MATLAB.

A shaker table has been used to provide excitation input at multiple amplitudes and multiple frequencies to the test setup. A shaker table manufactured by Unholtz Dickie (Model:

S452 LP) has been used to provide vibration input to the system. Figure 4.14 shows the shaker table along with the control unit.

Figure 4.14: Unholtz Dickie S452 LP shaker table and control unit.

The specification sheets of the test equipment used for experimentation are provided in Appendix A.

4.1.1 Data collection - flow diagram

The complete test setup used for this study consists of many different parts and pieces of technology working together. Figure 4.15 shows an overview in the form of a line diagram to demonstrate the flow of data collection, eventually stored in LabView.

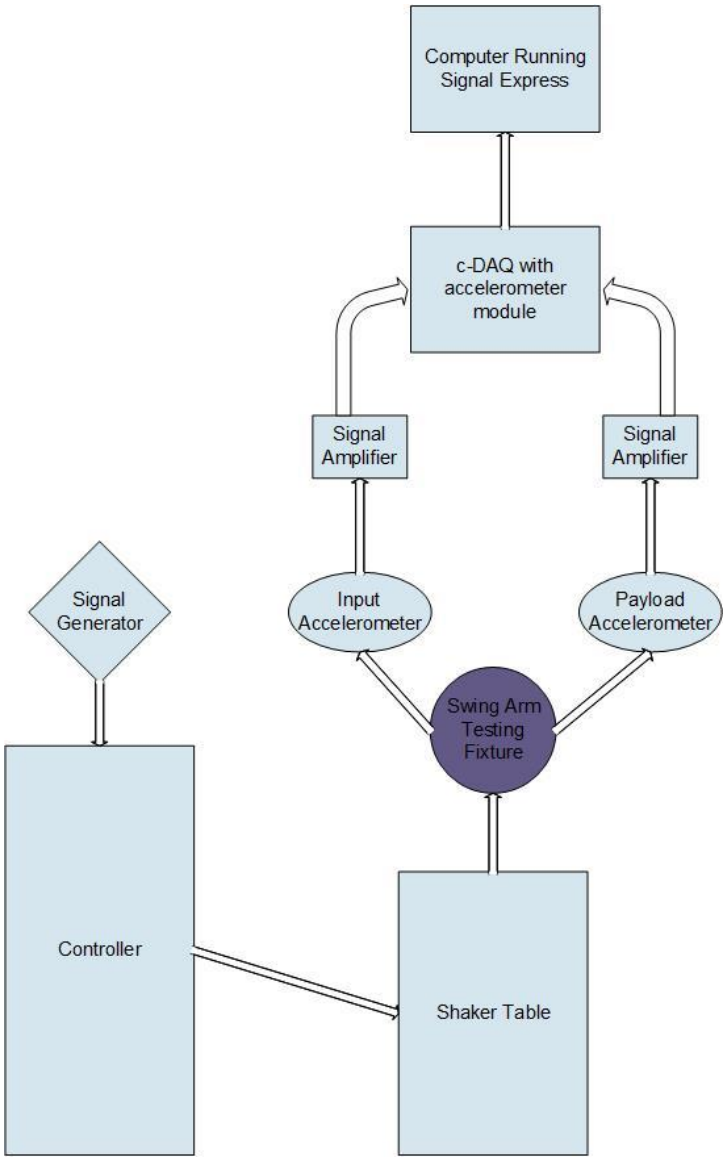

Figure 4.15: Test setup – line diagram.

As seen from the line diagram in Figure 4.15, a signal generator is used to input the required waveform. This allows the selection of frequency, frequency sweep, and amplitude of the input. This signal is used by the controller of the shaker table and provided as base excitation to the shaker table. The swing arm test fixture is assembled to the base plate of the shaker table

with accelerometers to measure the input and the output. The accelerometer signal is amplified by using the respective power amplifier units and then sent to the data acquisition unit.

Once the signal from the accelerometers is processed through the c-DAQ system and the accelerometer modules, the data is streamed to a laptop through LabView Signal Express. Each accelerometer data is collected through a separate channel and is saved individually in LabView.

Each channel of data can be individually inspected in LabView Signal Express to ensure that the data collection is operating smoothly. Once data collection is completed, all data is written to a .TDMS file that can be saved in a MS Excel file. Each data channel is written to a separate column along with a time stamp for each data point at a pre-determined frequency of data collection.

4.1.2 Data collection and processing

Once the raw data is collected and converted to a usable format, it needs to be processed into a meaningful format. The raw data is brought into MATLAB and typically post-processed, filtered, converted to frequency domain by using the Fast Fourier Transform and plotted. A MATLAB script has been written to perform all the post-processing operations.

The data is filtered by using a band-pass Butterworth filter. The cut-off frequencies of the filter are set iteratively to mitigate the low frequency and high frequency noise as per the explanation provided in Chapter 3. The Fast Fourier Transform (FFT) is used to transform the time domain data into the frequency domain. This is done to represent the input and output acceleration magnitudes in the frequency domain to assess vibration mitigation. A brief explanation of the Fourier transform and FFT is provided in Chapter 3.

The data collected in the time domain and converted to the frequency domain consists of thousands of data points. Although this data can be visually evaluated to qualitatively assess the

performance of the damper, this assessment may not be enough. As a result, the data is quantified by using the Root Mean Square (RMS) value as well as the peak values to quantitatively evaluate the performance of the damper. These values are used in conjunction with the qualitative assessment to analyze the damping results. Finally, multiple plots and graphs have been generated for each data set collected during testing. These figures are used to comprehend the performance of the damper and observe trends, if any. This is particularly important since there are a number of variables that can influence the performance of the damper. These figures and overall test results are presented in the next section, and relevant discussion is provided to explain and interpret the results.

4.2 Test Parameters

This section presents the test parameters along with the underlying reasons behind the choice of certain parameters that have been chosen for the test setup and test iterations. Results from the initial testing on the tensile tester are also presented. These results have been used for characterization of the damper parameters. This will be followed by the results from vibration testing using the two channel setup as well as the three channel setup.

4.2.1 Compression testing

Initial tests were performed using the tensile tester to determine the characteristics of the MR dampers used in this study. The two main tests that were performed included the first test at a constant rate of compression at 10 mm/min for a total stroke of 30 mm, and the second test that was performed at a constant force of 10N and for a total stroke length of 30 mm. These tests were performed at different current input to the electromagnet of the damper, controlled by the control kit of the damper. An example of the results can be seen in Figure 4.16.

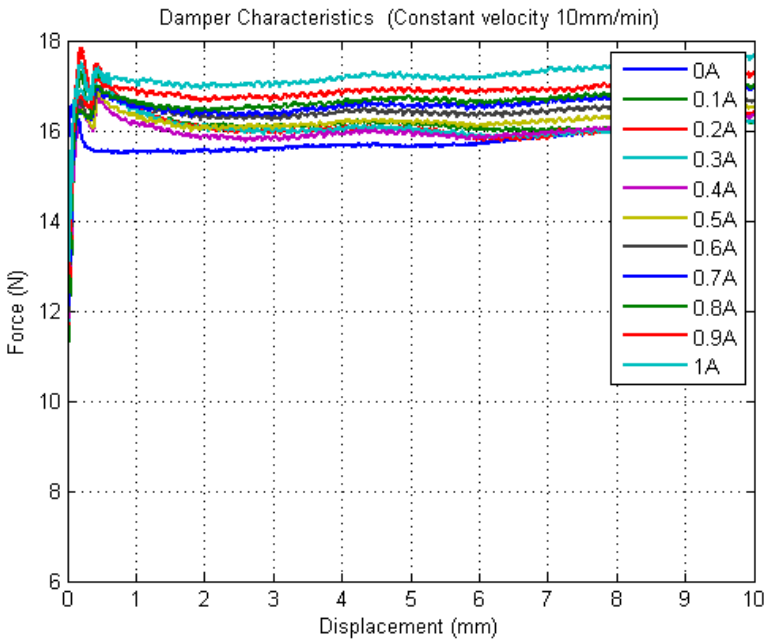

Figure 4.16: Force-displacement characteristics (at 10 mm/min).

These results provide a clear understanding of the variation of stiffness and damping characteristics of the damper as a function of the input current to the electromagnet of the damper. These test results are also useful for evaluating displacement and force transmissibility as a function of the input current for MR dampers.

4.2.2 Vibration testing

In order to develop an effective test plan, a list of the relevant parameters directly affecting the performance of the damping system was identified. A test matrix was developed in order to ensure that the most important test parameters would be represented in the test iterations. Table 4.1 shows the test matrix for the first round of testing that uses two accelerometers, one to measure the base input of the shaker table and another to measure the acceleration of the payload (representing the seating position on a motorcycle). Parameters such as vibration amplitude, excitation frequency, and current input are listed in Table 4.1.

Table 4.1: Test matrix – 2 channel testing.

Frequency Sweep 5 - 100Hz				
Current input (A)	Amplitude			
	Base	Payload	Base	Payload
	150mVpp	150mVpp	450mVpp	450mVpp
0.0				
0.1				
0.2				
0.3				
0.4				
0.5				
0.6				
0.7				
0.8				
0.9				
1.0				

Three accelerometers were used in the second round of testing. While the accelerometer on the shaker table measures the base excitation, the second accelerometer is mounted at the top of the damper and the third accelerometer is attached to the frame at a location representing the position of a rider's foot peg on the motorcycle. The test matrix for this second round of testing is presented in Table 4.2.

Table 4.2: Test matrix – 3 channel testing.

Frequency Sweep 5 - 100Hz						
Current input (A)	Amplitude					
	Base	Foot Peg	Damper	Base	Foot Peg	Damper
	150mVpp	150mVpp	150mVpp	450mVpp	450mVpp	450mVpp
0.0						
0.5						
1.0						

The two test matrices include all parameters that have been identified as critical variables that affect the performance of the damping system from previous test results and literature

review. Two amplitudes have been used during testing to comprehend the influence of excitation amplitude. These two amplitudes are seen to be significant for displacement excitation of the shaker table top. The semi-active nature of the MR damper is its most attractive feature, therefore the input current to the electromagnet of the damper is used as the control variable for the damper. From the compression testing of the MR dampers used for this study, 0A to 1A is seen as the most useful range of input current. For the first round of testing, an increment of 0.1A is used to comprehend the sensitivity of the damper characteristics to the changing current. For the second round of testing, this increment has been changed to 0.5A since a sufficient amount of data is available from the first round of data collection.

A frequency sweep of 5 – 100Hz is carefully selected to strike a balance between the use of the damping system in a motorcycle system and the capability of the testing system. For a general motorcycle rear suspension system used in normal operating conditions at low, medium and high speeds, a frequency range of 5 – 100 Hz sufficiently encompasses the majority of frequencies that the damping system may be exposed to on different terrains [4].

It may be noted that some initial testing trials were performed at individual excitation frequencies, and small frequency ranges such as 5 – 30Hz, etc. After conducting these trials, it was decided to use large frequency sweeps to limit the iterations of data collection while evaluating the necessary attributes of the suspension system without having an overload of data.

4.3 Damping Results

This section presents all the results from the vibration testing performed for this study. The data collected during testing is summarized in the form of time history and frequency response plots, some bar graphs and trends are also presented to discuss the results. It may be

noted that the results presented in this section represent a portion of all the data collected for this study to highlight the main findings concisely.

4.3.1 Two channel test results

The data collected from each set of parameters has been processed by using a MATLAB script. Some of the results shown in this section are from a test run conducted at an input current of 0.2 A with a peak-to-peak excitation amplitude of 450 mV and an excitation frequency ranging from 5 to 100 Hz.

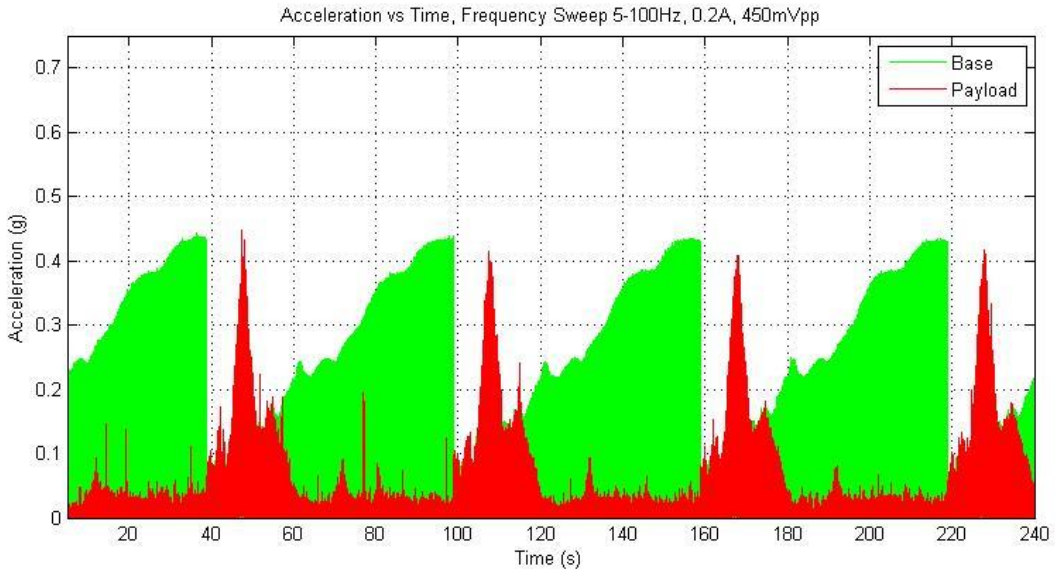

Figure 4.17: Acceleration time history, damper current 0.2A, frequency sweep 5 Hz - 100Hz, amplitude 450 mVpp.

Figure 4.17 shows the time history of the data collected without any post-processing. A 60 second cycle time can be clearly discerned from Figure 4.17 with 4 distinct cycles. This plot presents the base acceleration that is measured from the shaker table and the payload acceleration measured from a specific location on the swing arm. Acceleration is recorder in 'g' units with 1 g = 9.81 m/s^2. It is common practice to present acceleration data in these units. It can be seen from Figure 4.17 that there are some frequencies at which the damper mitigates vibration with the

payload amplitude being significantly smaller than the base amplitude. However, there are some instances where the payload amplitudes are significantly high with the damper being unable to mitigate vibrations.

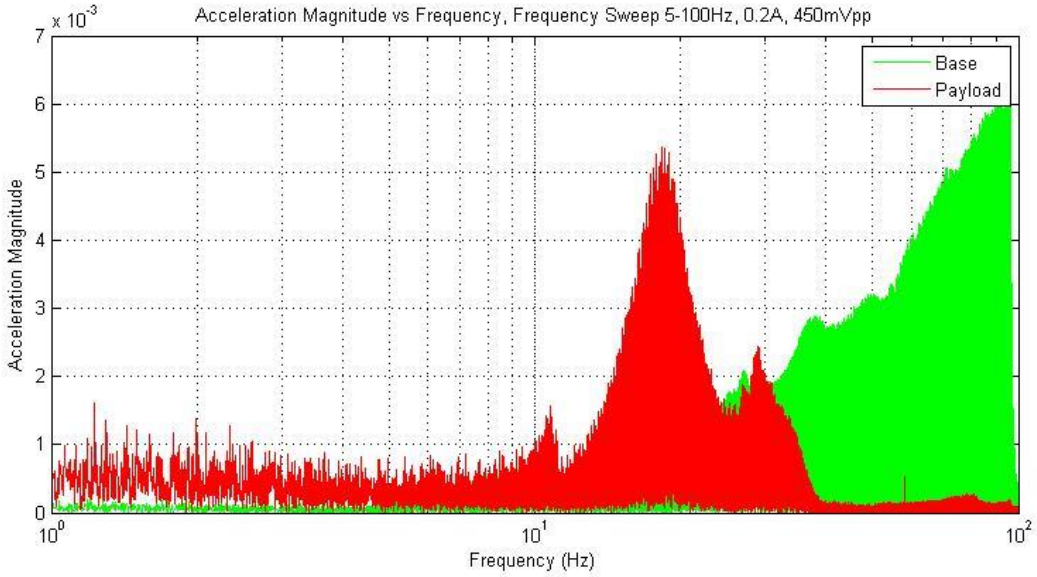

Figure 4.18: Acceleration frequency response, damper current 0.2A, frequency sweep 5Hz - 100Hz, amplitude 450 mVpp.

Figure 4.18 shows the frequency response for the time history shown in Figure 4.17. This plot shows the magnitude of acceleration versus frequency. The acceleration magnitude clearly shows the frequency range over which the damper is able to mitigate vibration as well as the range over which the damper is unable to prevent the payload from an amplification of input acceleration. Visual inspection of this plot confirms that there is little excitation below 10 Hz, while there is a significant amplification of payload response from 10Hz to 35Hz with two distinct peaks around 20Hz and 30Hz. These peaks are seen repeatedly in multiple tests, and correspond to the resonant frequencies of the system. Above 35Hz, the acceleration magnitude of the payload is seen to drop off drastically as the acceleration magnitude of the base input continues to increase. A similar general behavior has been observed over most of the test runs,

with an observed difference in the location of amplification peaks, acceleration magnitudes, and amount of damping.

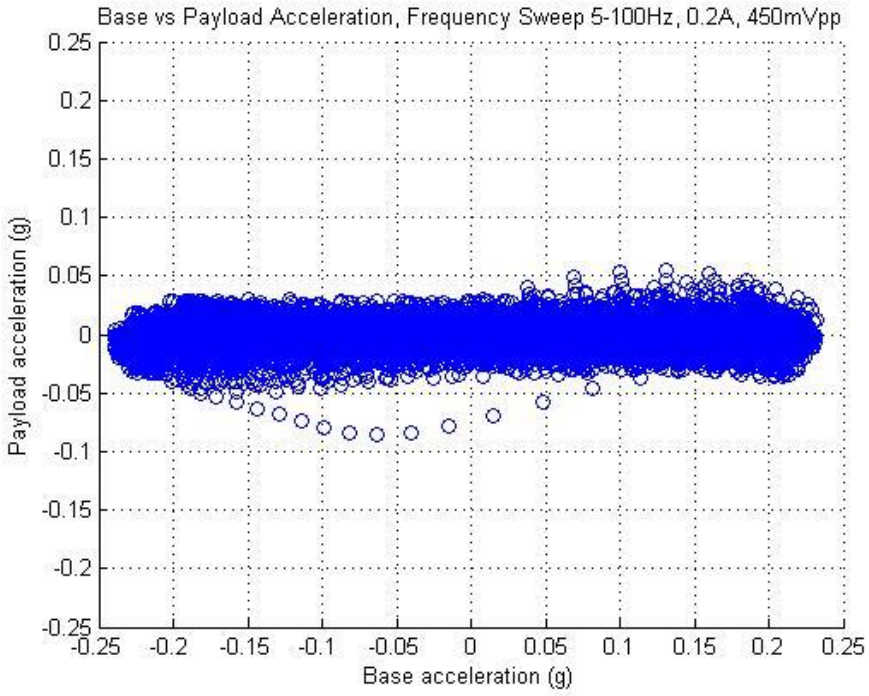

Figure 4.19: Payload acceleration versus base acceleration, damper current 0.2A, frequency sweep 5Hz - 100Hz, amplitude 450 mVpp.

Figure 4.19, the final plot from this test is generated in the form of payload acceleration versus base acceleration, otherwise known as a hysteresis plot. This plot shows the full range of accelerations for the base and the payload. The orientation of the hysteresis loop is relatively flat, indicating a small phase angle and a relatively small damping ratio. This can be attributed to the low input current to the electromagnet for this test run. This will be discussed further in the other hysteresis loops presented in this section.

Figures 4.20 through 4.22 show results from another iteration of data collection. All parameters are identical to the previous iteration except for the input current to the electromagnet, that has been increased to 0.9 A (from 0.2 A). Figure 4.21 shows the time history

of acceleration of the base as well as the payload. Some spikes can be noticed in the time history plot, these could be attributed to noise. Noise has been filtered out by using a band pass filter before plotting the frequency response. The frequency response for this iteration is shown in Figure 4.21.

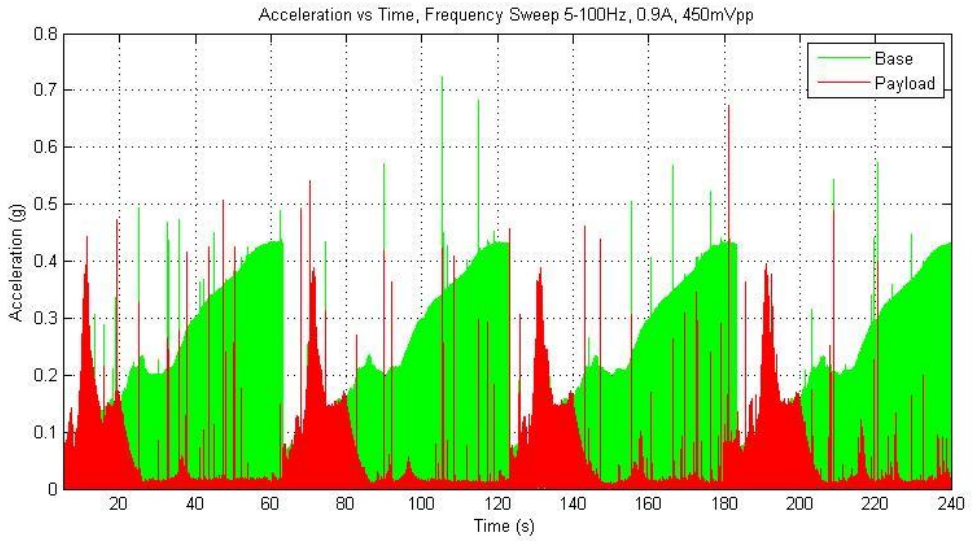

Figure 4.20: Acceleration time history, damper current 0.9A, frequency sweep 5Hz - 100Hz, amplitude 450 mVpp.

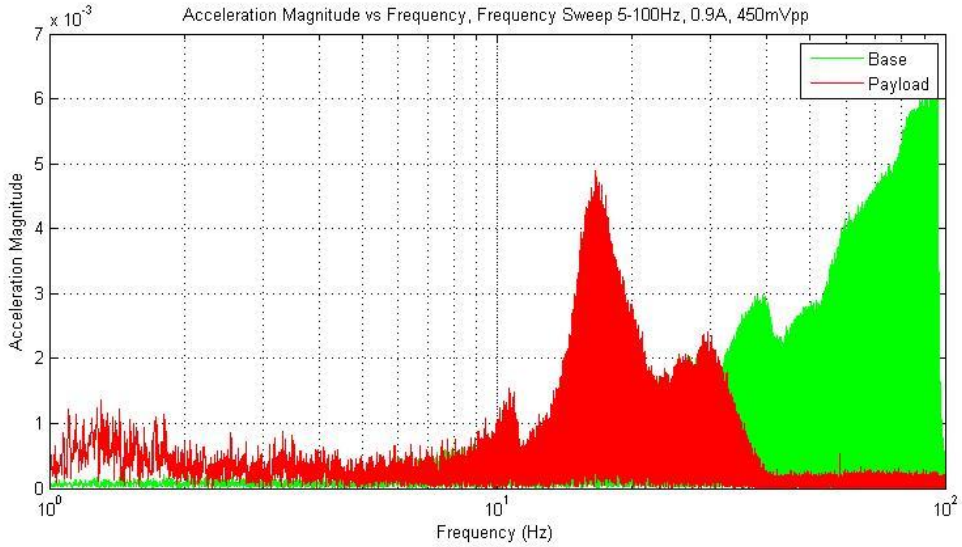

Figure 4.21: Acceleration frequency response, damper current 0.9A, frequency sweep 5Hz - 100Hz, amplitude 450 mVpp.

Figure 4.22 shows the hysteresis plot for the results from the second iteration. In comparison to the results in Figure 4.19, it can be seen that the orientation of the hysteresis loop changes from around 3 deg. to approximately 80 deg. This indicates enhanced damping at an input current of 0.9 A to the electromagnet of the damper.

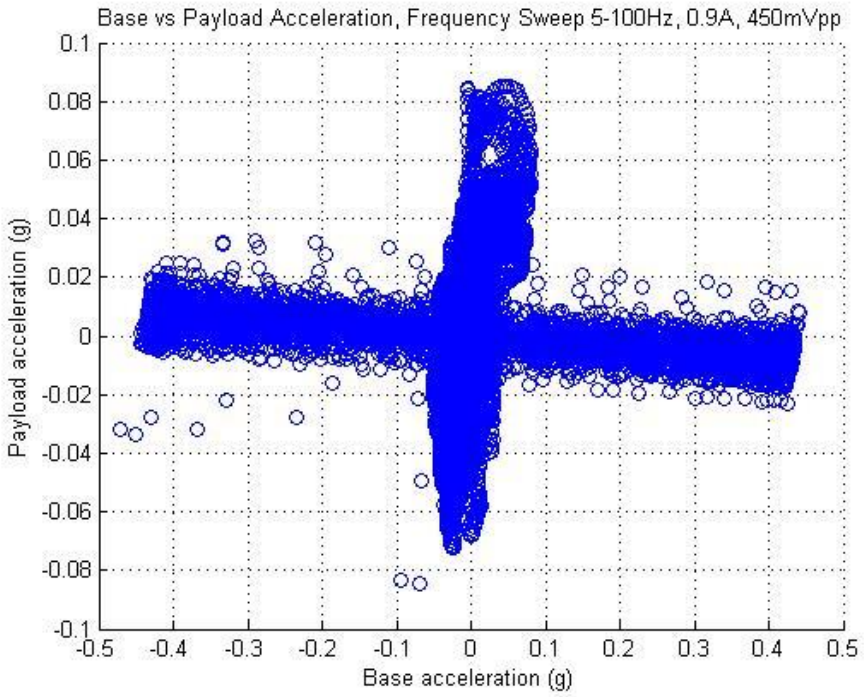

Figure 4.22: Payload acceleration versus base acceleration, damper current 0.9A, frequency sweep 5Hz - 100Hz, amplitude 450 mVpp.

Although there may not be much visual difference between the two data sets presented thus far, the time history and frequency response are seen to change significantly with the changing parameters and the varying levels of damping. In order to quantitatively compare the results, the root mean square (RMS) and the maximum (Max) values of acceleration are tabulated. One such result is shown in Table 4.3.

Table 4.3: Comparison – base versus payload acceleration.

Frequency Sweep 5 - 100Hz					
Input current (A)		Acceleration (g)			
		Base	Payload	Base	Payload
		150mVpp	150mVpp	450mVpp	450mVpp
0.0	RMS	0.0578	0.0299	0.1894	0.0561
	Max	0.3584	0.6594	0.7055	0.4040
0.1	RMS	0.0589	0.0292	0.1926	0.0637
	Max	0.5109	0.4607	0.6908	0.4081
0.2	RMS	0.0613	0.0363	0.1955	0.0702
	Max	0.5000	0.8382	0.4424	0.4481
0.3	RMS	0.0611	0.0286	0.1946	0.0709
	Max	0.1554	0.2826	0.7036	0.4230
0.4	RMS	0.0619	0.0279	0.1930	0.0742
	Max	0.3780	0.3902	0.5123	0.4804
0.5	RMS	0.0604	0.0305	0.1933	0.0703
	Max	0.2253	0.3008	0.4448	0.4181
0.6	RMS	0.0601	0.0257	0.1957	0.0688
	Max	0.2468	0.1860	0.7467	0.5860
0.7	RMS	0.0599	0.0274	0.1911	0.0672
	Max	0.5634	0.4928	0.7520	0.6109
0.8	RMS	0.0604	0.0265	0.1919	0.0646
	Max	0.5847	0.5555	0.8205	0.5015
0.9	RMS	0.0603	0.0258	0.1921	0.0655
	Max	0.6079	0.4961	0.7239	0.6735
1.0	RMS	0.0615	0.0297	0.1946	0.0684
	Max	0.4186	0.4608	0.8428	0.6265

In order to easily discern the results listed in Table 4.3, bar graphs are used to visualize the trends in acceleration as the input current to the electromagnet of the damper is varied. Figures 4.23 and 4.24 show two such bar graphs for two different excitation amplitudes using the data from Table 4.3.

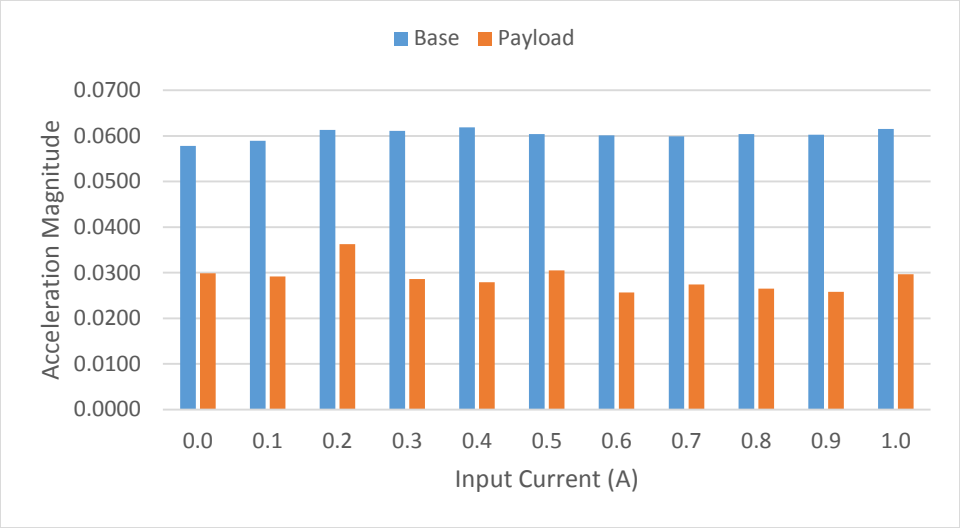

Figure 4.23: Base versus payload RMS values at 150mVpp.

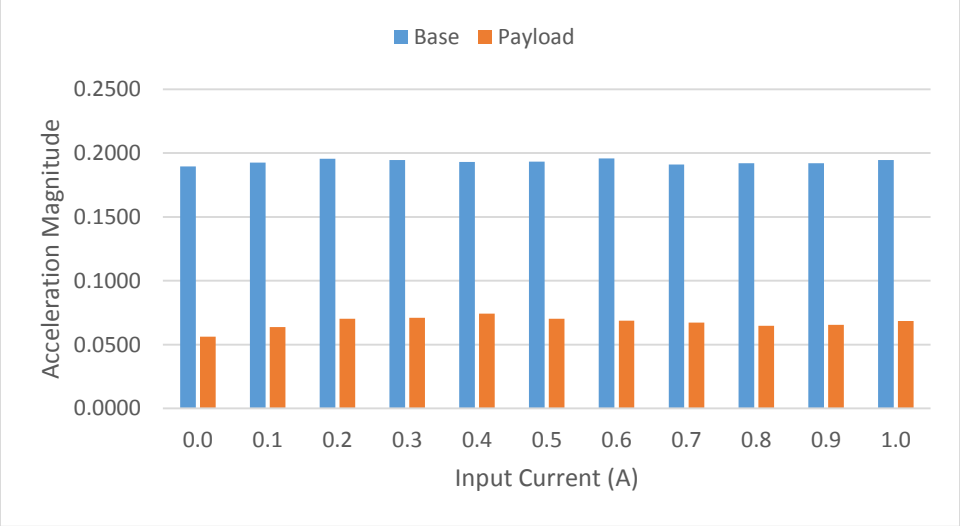

Figure 4.24: Base versus payload RMS values at 450mVpp.

Figures 4.23 and 4.24 clearly indicate vibration mitigation since the payload acceleration (RMS) is significantly lower than the base acceleration. It may be noted that the RMS is an average value that represents the entire data as one number. As the input current to the electromagnet increases, the MR damper exhibits an increase in damping. This is expected to

result in a proportional reduction in the acceleration of the payload over the time history. This can be seen clearly from Figure 4.25, where the difference in RMS acceleration is plotted. An incremental trend is seen in the reduction of acceleration (from the base to the payload) with the increase in the input current. However, this incremental trend is not evident when the excitation amplitude increases, as seen in Figure 4.26.

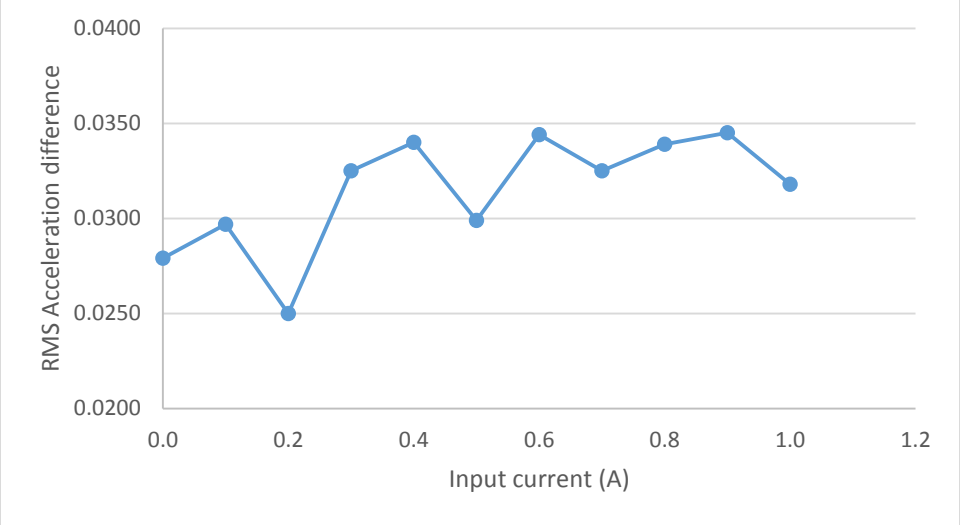

Figure 4.25: RMS acceleration difference (base-payload) at 150mVpp.

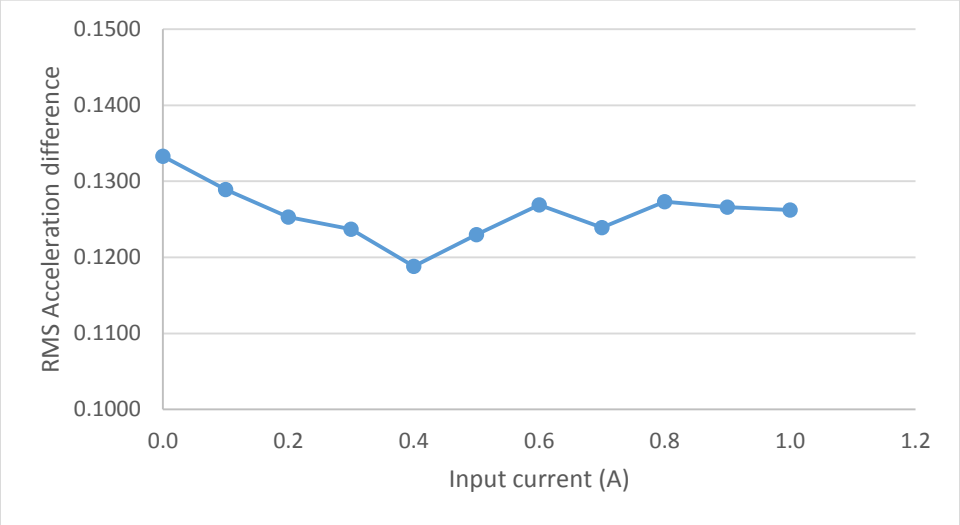

Figure 4.26: RMS acceleration difference (base-payload) at 450mVpp.

Another method of interpreting the data is to look at the peak acceleration values from the frequency response. Figures 4.27 and 4.28 show a comparison of the maximum acceleration amplitudes in the frequency domain.

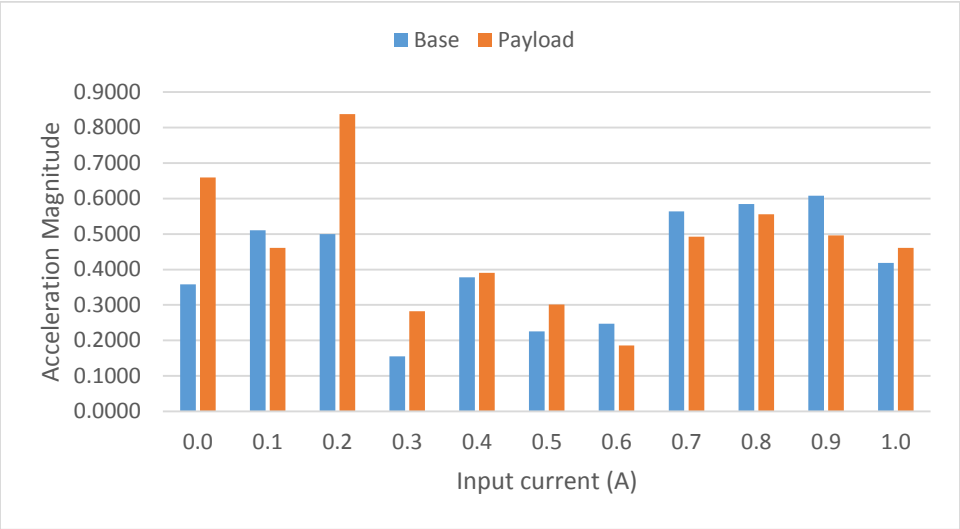

Figure 4.27: Base versus payload MAX values at 150mVpp.

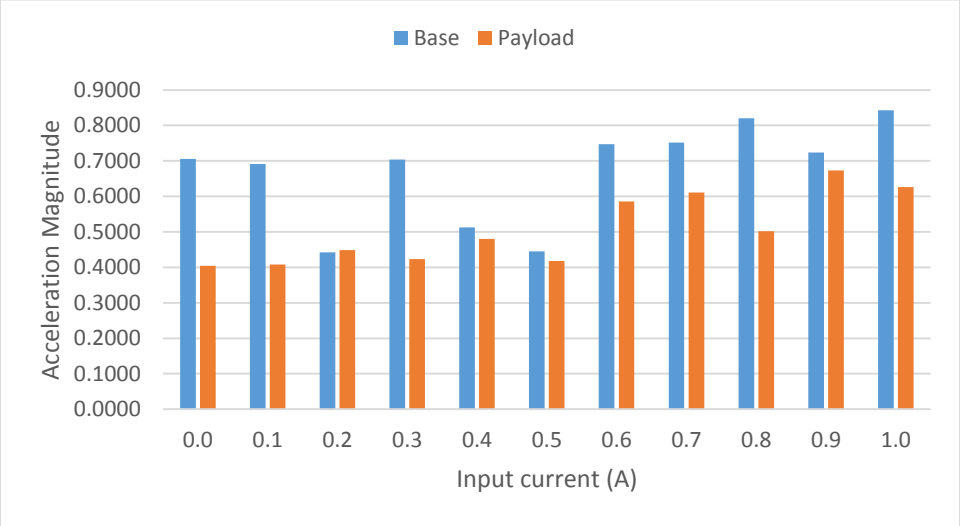

Figure 4.28: Base versus payload MAX values at 450mVpp.

Maximum acceleration amplitude is not a robust indicator of vibration mitigation, as can be seen from the results in Figures 4.27 and 4.28. This is primarily because of the resonance peaks leading to a high amplification of the input excitation at one specific instance, as seen in some of the results in Figure 4.27. This shortcoming has been overcome by using the RMS values of acceleration, in addition to the peak values, in order to assess vibration mitigation over the entire time history rather than one specific amplitude.

4.3.2 Three channel test results

For the second round of testing, two accelerometers have been used to measure vibrations at two locations of the swing arm – one directly above one of the dampers and the other approximately at the location of the rider foot peg on a motorcycle. The base excitation has been measured as in the first round of testing. Figures 4.29 and 4.30 show time history and frequency response from the three channels of data.

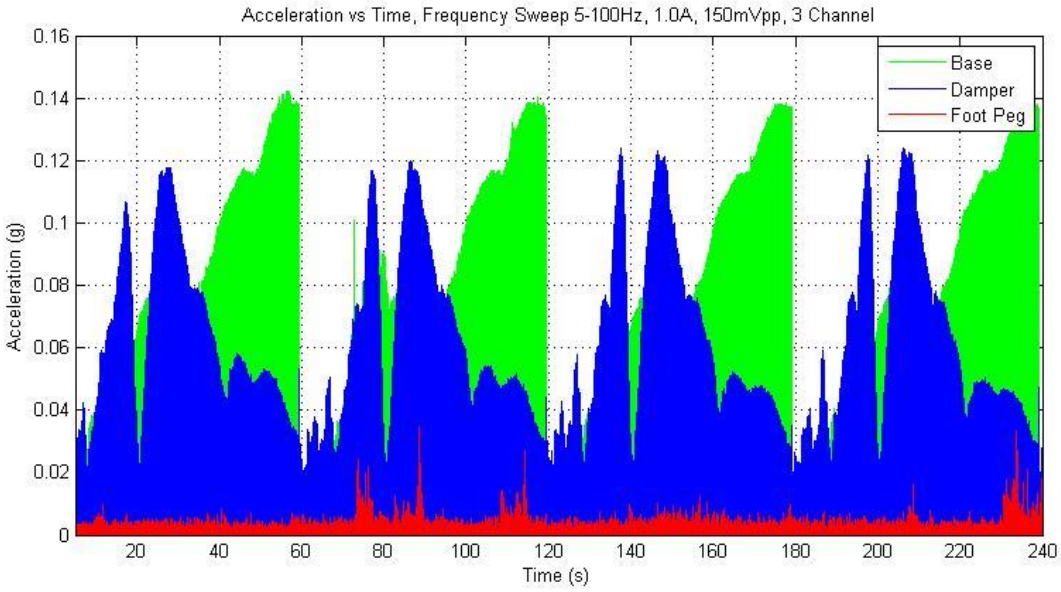

Figure 4.29: Acceleration time history (3 channels), damper current 1.0A, frequency sweep 5Hz - 100Hz, amplitude 150 mVpp.

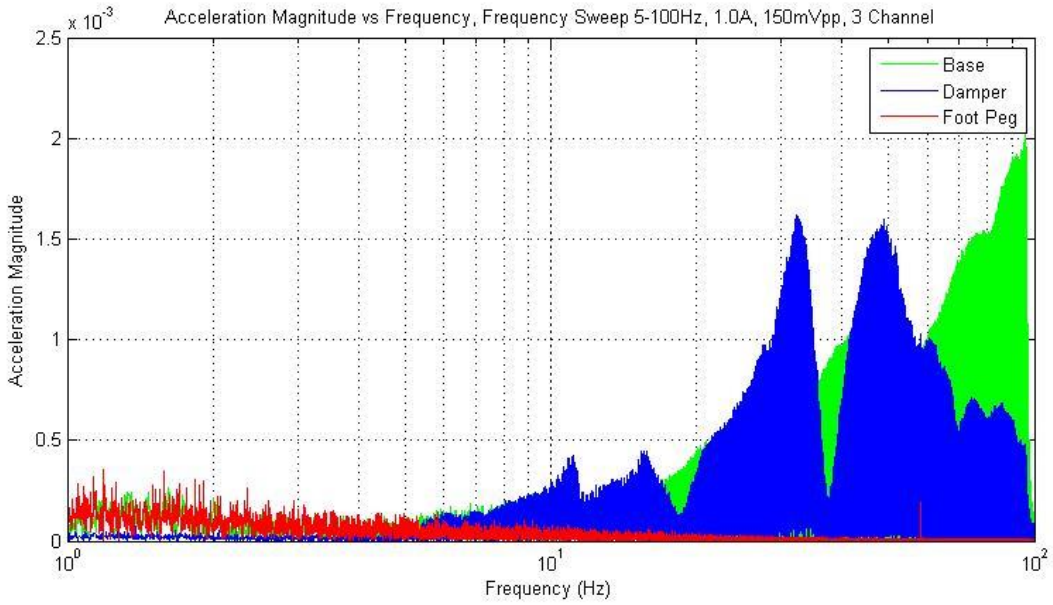

Figure 4.30: Acceleration frequency response (3 channels), damper current 1.0A, frequency sweep 5Hz - 100Hz, amplitude 150 mVpp.

Figures 4.29 and 4.30 both indicate that the foot peg location exhibits a significant amount of mitigation. The other location at the damper exhibits similar results to the payload from the first round of testing. Figures 4.31 and 4.32 demonstrate the hysteresis plots for the two locations on the swing arm.

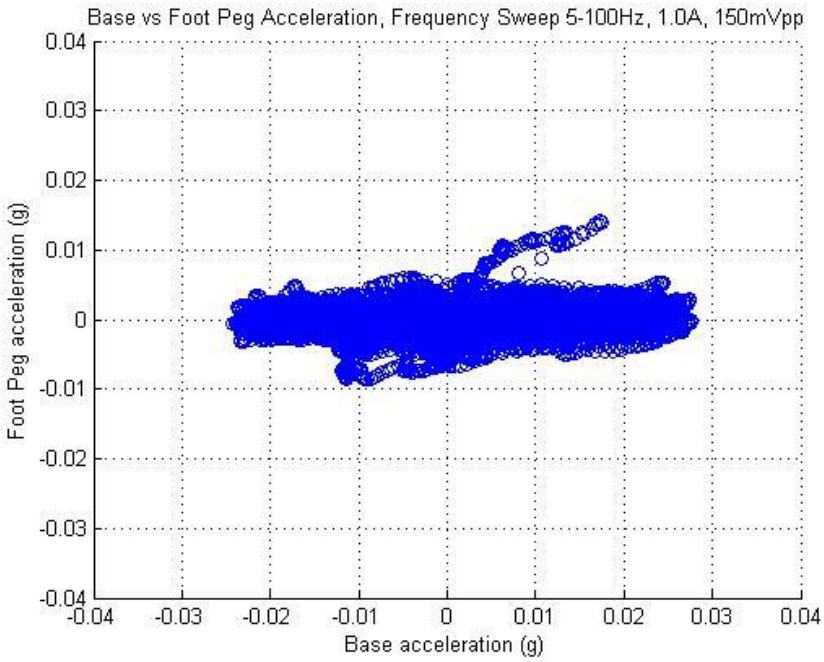

Figure 4.31: Foot peg acceleration versus base acceleration, damper current 1.0A, frequency sweep 5Hz - 100Hz, amplitude 150 mVpp.

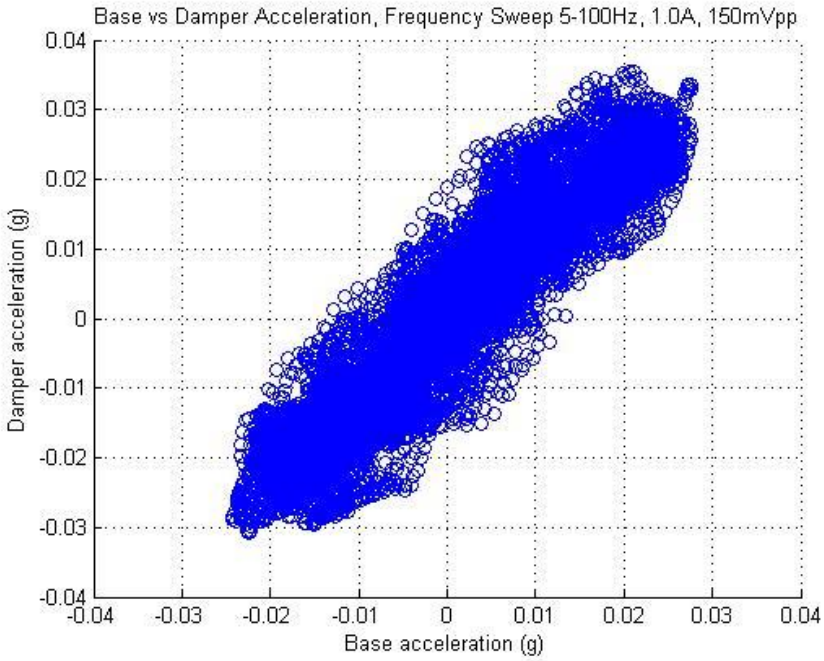

Figure 4.32: Damper acceleration versus base acceleration, damper current 1.0A, frequency sweep 5Hz - 100Hz, amplitude 150 mVpp.

As can be seen from Figures 4.31 and 4.32, the area enclosed by the acceleration hysteresis plots as well as the orientation of hysteresis is significantly different between the two locations. This indicates a significant difference in frequency response between the two locations.

Only three current inputs were used for the second round of testing in order to get an overall understanding of the performance of the suspension system with different locations of accelerometers. Similar to the previous iteration, the RMS and peak values of acceleration are identified and have been listed in Table 4.4.

Table 4.4: Comparison – base versus foot peg/damper acceleration.

Frequency Sweep 5 - 100Hz							
Current Input (A)		Amplitude (g)					
		Base	Foot Peg	Damper	Base	Foot Peg	Damper
		150mVpp	150mVpp	150mVpp	450mVpp	450mVpp	450mVpp
0.0	RMS	0.0571	0.0018	0.0390	0.1863	0.0013	0.0696
	Max	0.1595	0.0207	0.1178	0.4900	0.0144	0.2065
0.5	RMS	0.0592	0.0030	0.0470	0.1892	0.0038	0.1030
	Max	0.1583	0.0421	0.1357	0.4324	0.0562	0.4284
1.0	RMS	0.0587	0.0028	0.0443	0.1929	0.0024	0.1079
	Max	0.1423	0.0345	0.1241	0.4284	0.0235	0.5156

This data is plotted in Figures 4.33 through 4.36 for a visual comparison. The RMS values of acceleration are plotted in Figures 4.33 and 4.34, and the maximum values are plotted in Figures 4.35 and 4.36.

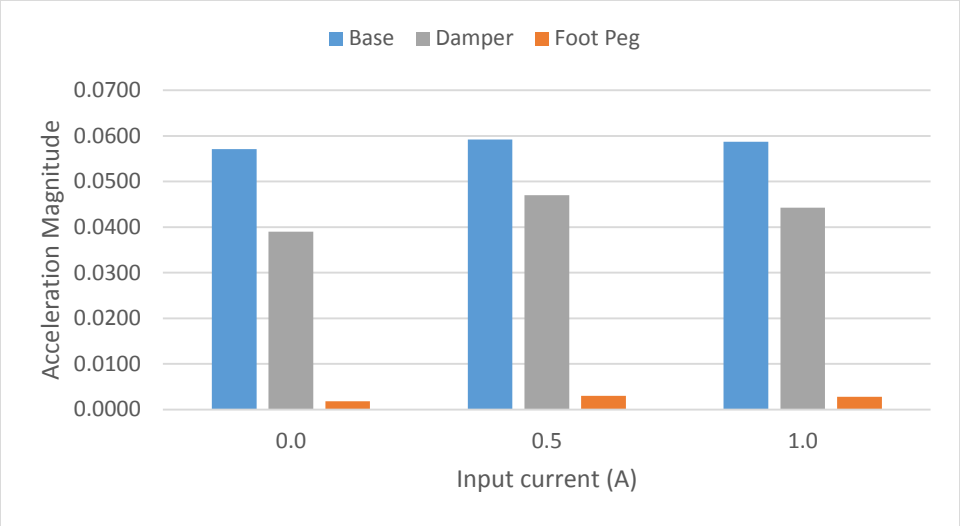

Figure 4.33: Base, damper and foot peg acceleration (RMS) at 150mVpp.

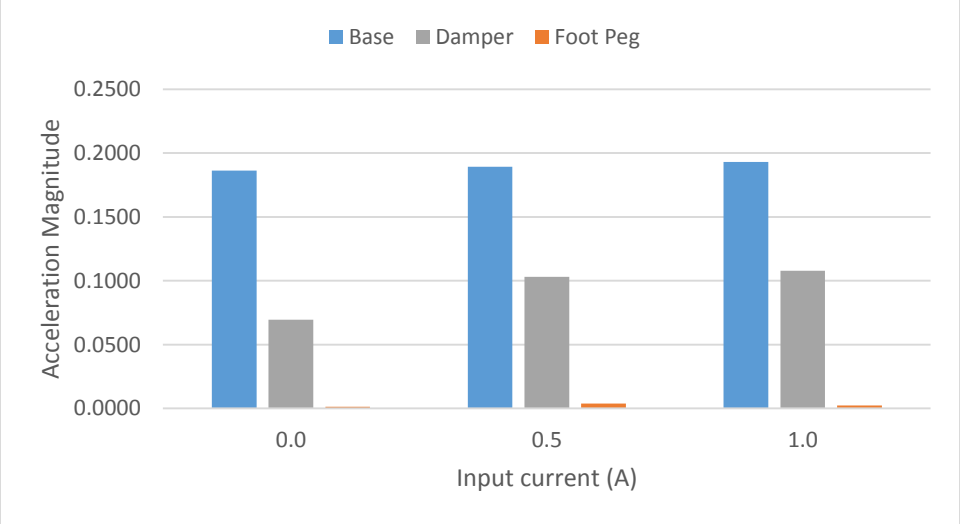

Figure 4.34: Base, damper and foot peg acceleration (RMS) at 450mVpp.

The RMS values in Figures 4.33 and 4.34 clearly demonstrate a high level of vibration mitigation at both levels of excitation.

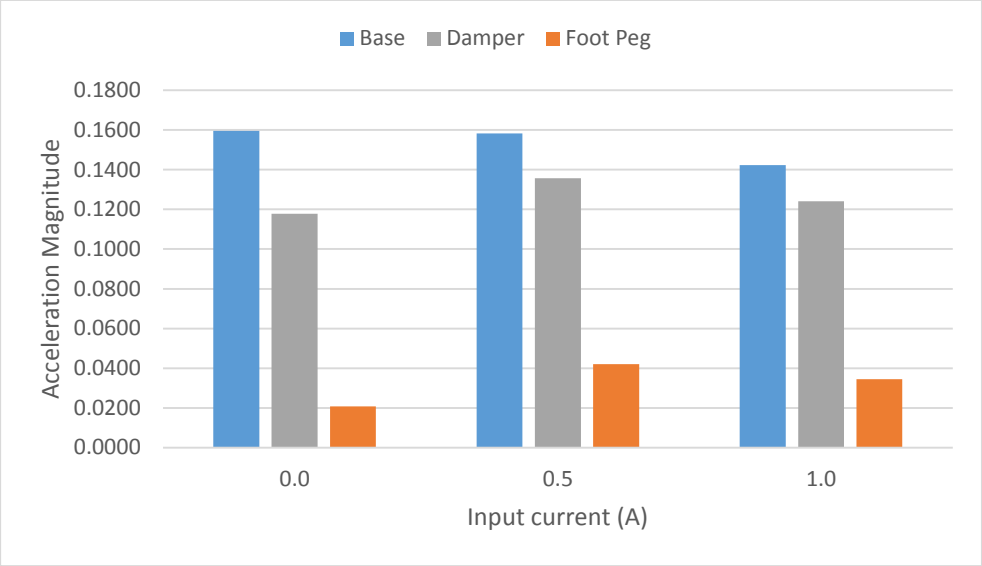

Figure 4.35: Base, damper and foot peg acceleration (Max) at 150mVpp.

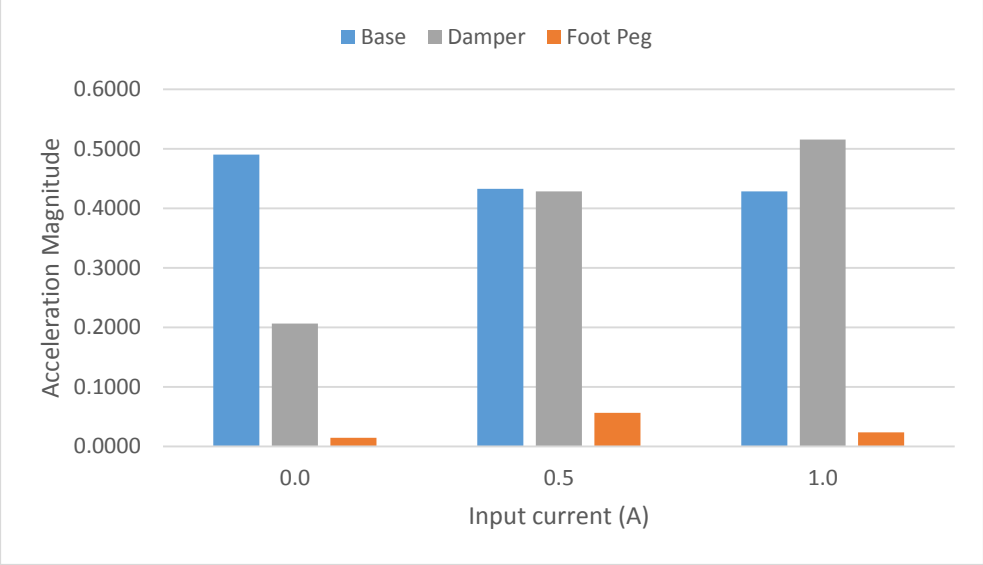

Figure 4.36: Base, damper and foot peg acceleration (Max) values at 450mVpp.

The comparison of the maximum levels in Figures 4.35 and 4.36 still indicates significant mitigation at the foot peg location. However, the second location shows poor mitigation at higher amplitudes of excitation and higher input current to the electromagnet.

4.4 Conclusions

The experimental setup, the fixture design and the data collection have been presented in this chapter. Two rounds of data collection have been performed to evaluate vibration mitigation at different locations of the swing arm. The data has been post-processed and analyzed, and conclusions have been drawn about the performance of the damper. An overview of the equipment used for this study has also been included in this chapter.

Results indicate that RMS acceleration is significantly mitigated at multiple locations of the swing arm. Also, the foot peg location on the swing arm shows particularly high levels of mitigation in terms of RMS acceleration as well as maximum acceleration. The semi active nature of the damper allows for direct control of damping by changing the input current to the electromagnet of the damper.

The next chapter, Chapter 5, will present overall conclusions from this research. The application of MR dampers in a motorcycle swing arm system is particularly discussed in the next chapter. Future scope of this study has also been discussed in the next chapter.

CHAPTER 5: CONCLUSIONS AND FUTURE RESEARCH

Traditional passive dampers play a vital role in vehicle suspension systems. They isolate the main body of the vehicle and its occupants from undesirable vibrations and potentially harmful sudden forces. However, as with all technologies there is always room for improvement and enhancement. One limitation of passive dampers is they must be set to a single stiffness and damping which is primarily determined by the main use of that damper. These settings can be simplified to a relatively soft and compliant system for improved comfort, but relatively poor handling. On the other hand, a relatively stiff system with high damping improves handling at the expense of reduced ride comfort. Active and semi-active dampers seek to solve this problem of having only one setting of stiffness and damping for the damper.

5.1 Summary

This research has been focused on an investigation into the application of semi-active MR dampers for use in a motorcycle (rear) swing arm suspension system. This research primarily focused on a traditional swing arm set up with dual shocks, and the experimental work was carried out to quantify vibration mitigation with an MR damping system.

The first phase of this study involved researching the current literature on motorcycle suspensions, MR fluid and dampers, and the application of MR and other semi-active dampers on suspensions. The second phase of this research was to investigate the transmissibility and characteristics of the MR dampers used in this study. This was accomplished by compression testing, and recording and analyzing the test results. Methods for post processing the vibration testing data by filtering and obtaining a frequency response was researched and reviewed. Three

mathematical models that can be used to demonstrate the dynamic characteristics of the swing arm system were developed and presented. This phase also included investigation into a skyhook control algorithm, and simulated results from this system were used in this research.

The third phase of this research involved design, fabrication, and testing of a motorcycle swing arm suspension system through the use of a fixture that represented the key characteristics of this system. A lightweight design that sufficiently simulated the dynamics of a traditional dual shock rear swing arm was developed. The test fixture was fabricated and assembled on a vibration (shaker) table. All data collection equipment was incorporated with the fixture and test set up.

The final phase of this research was to run tests at predetermined parameter settings, collect data from testing, process data, and analyze the results. The data was presented in a comprehensive discussion comparing the multiple parameters and their effect on the outcome. Acceleration data was obtained across the base input of the swing arm and compared to the accelerations at payload locations and a few other locations on the fixture.

5.2 Conclusions

The main conclusion from this research is that a significant change in the system dynamics can be observed by altering the settings of the MR dampers. As concluded in Chapter 4, the dual damper swing arm with MR dampers provides vibration mitigation at multiple locations of the frame. Therefore, the use of MR dampers in the swing arm system is viable. Data indicates that the payload is isolated through the entire range of all current settings of the damper, and the performance of the damper is seen to be robust. The mitigation in RMS

acceleration is seen to range from 51.2% to 80.2% for 150mVpp amplitude and 88.9% to 108.6% for 450mVpp amplitude.

The second round of experiments involved the measurement of acceleration at other key locations such as rider seat position and the foot peg location. The rider foot peg location is a key point of interest when detecting vehicle vibration since high vibrations are known to induce rider fatigue since the foot peg is a major point of contact between the rider and the frame of the motorcycle. These tests reveal that the foot peg is significantly isolated from vibrational inputs at the rear axle at multiple amplitudes of excitation through a large range of excitation frequencies. Mitigation levels in RMS acceleration at the foot peg range from 180.7% to 187.8% for 150mVpp amplitude, and 192.1% to 197.2%.for 450mVpp amplitude.

It is important to note that a comparison of the maximum values of acceleration from testing data does not always accurately indicate the levels of vibration mitigation. In some test results it can be seen that the payload values exceed the base values of acceleration at a specific frequency of excitation. This is due to the inherent natural frequencies of the system causing the payload to reach higher acceleration values at one specific frequency. Under normal operating conditions, the natural frequency of any system is avoided by attempting to maintain normal operation frequencies outside of the amplification range. The frequency range for this study has been maintained from 5Hz to 100Hz. This range has been used since it represents a wide variety of road conditions, ranging from off road or cobble stone road, where frequency is very low with high amplitude, to a smooth pavement where frequency is very high but with a low amplitude.

Another key observation from this study is that a change in the natural frequency of the system is detected as the current input to the electromagnet is changed. When reviewing the data

from all testing runs, the mean value of the natural frequency is seen to range from 16Hz to 19Hz, with the higher values of input current resulting in higher natural frequencies.

This is an important observation since this can be seen to provide the MR damping system another potential advantage over a passive damping system. Due to this phenomenon, the natural frequency of the rear suspension can be avoided by the development of an appropriate control algorithm that uses the current input to the damper as the control parameter. Further studies must be done at full scale to determine if this characteristic of MR dampers can be used in a complete suspension system.

Although the results of this study are preliminary and have been limited to a mock representation of a rear swing arm suspension system, the observations from the experimental evaluation are directly applicable to the rear suspension of a motorcycle. The results from this study indicate that the MR dampers provide a viable opportunity from improving motorcycle suspension that can be controlled. The prospect of implementing MR dampers into a motorcycle suspension presents many valuable possibilities for improving motorcycle dynamics, rider satisfaction, and overall handling.

5.3 Future Scope

While this study investigates the feasibility of applying MR dampers to a rear swing arm suspension system, there are many areas of future scope that can be studied. A direct continuation of the work presented in this thesis could include improving the testing fixture and adding a representation of the tire patch by including an unsprung mass to the testing set up. An improved testing setup would provide a better understanding of the MR damping characteristics for the swing arm suspension but the fixture would be slightly more complex. Including a tire

patch and unsprung mass in the testing fixture introduces more variables that can be altered, and will provide more insight into the overall dynamic behavior.

A second means of improving the test fixture is to scale up the set up and include coil springs to the system to completely represent the spring-damper units. This will provide experimental data that is closer to the real-world application while still being able to conduct vibrational analysis in a controlled environment.

An obvious area for future work would be to adapt a functioning motorcycle to operate with MR dampers. The system would be fitted with instrumentation to observe how MR dampers will respond under road conditions with varying riding styles. Tests can be conducted at preset damper settings to determine the performance of the damper.

This study analytically investigates the use of a skyhook control algorithm in a swing arm suspension system. Future studies can continue to develop an applicable control algorithm and test its feasibility to actively mitigate vibrations with the input current as the control variable. A final possibility for applying semi-active dampers to a motorcycle suspension could be to investigate the feasibility of altering the damping settings of a motorcycle based on lean angle and lateral directional forces to improve handling and ride comfort. By stiffening the suspension system of the motorcycle in a cornering maneuver and softening the system during straight line riding, semi-active dampers can actively improve riding dynamics and rider comfort of a motorcycle.

Semi-active and active suspension systems are an exciting field of research that present possibilities to improve a technology that affects nearly everyone who drives a vehicle. Investigating these possibilities is unquestionably a worthwhile endeavor.

BIBLIOGRAPHY

[1] Carlson, J. D., Weiss, K. D., 1994, A growing attraction to magnetic fluids, *Machine Design, Vol. 66*, No. 15, p. 61-64.

[2] Chen, C., 2001, Digital signal processing: Spectral computation and filter design. Oxford, New York: Oxford University Press.

[3] Cocco, G., 2004, Motorcycle design and technology. St. Paul, MN: Motorbooks International.

[4] Gordon, T., & Bareket, Z., 2007, Vibration Transmission from Road Surface Features – Vehicle Measurement and Detection, Technical Report, The University of Michigan Transportation Research Institute (UMTRI).

[5] Gravatt, J., 2003, Magneto-Rheological Dampers for Super-sport Motorcycle Application, Master's Thesis, Virginia Polytechnic Institute and State University, Blacksburg, VA.

[6] Harris, C., 2002, APPENDIX 1.2 TERMINOLOGY. Harris' shock and vibration handbook, 5th ed., New York: McGraw-Hill.

[7] Longhurst, C., 2014, The Motorbike Suspension Bible. Retrieved September 21, 2015, from http://www.carbibles.com/suspension_bible_bikes.html

[8] Lord Corporation, www.lord.com

[9] Mark R., Jonathan W., & Carlson J. Properties and Applications of Commercial Magnetorheological Fluids. In Coe. Montana. Retrieved February 26, 2012, from http://www.coe.montana.edu/me/faculty/jenkins/Smart%20Structures/prop%20MRF.pdf

[10] MathWorks Inc. Documentation Fast Fourier transform. Retrieved October 12, 2015, from http://www.mathworks.com/help/matlab/ref/fft.html

[11] Newport Corporation, Fundamentals of Vibration. Retrieved October 12, 2015, from http://www.newport.com/Fundamentals-of-Vibration/140234/1033/content.aspx

[12] Pare, C. A., 2000, A Quarter-Car Experimental Analysis of Alternative Semiactive Control Methods, *Journal of Intelligent Materials Systems and Structures*, 11, pp. 604-612.

[13] Sarigul-Klijn, N., Lopez, I., Sarigul-Klijn, M., Karnopp, D., 2007, Vibration Mitigation Using Passive Active Tunable (PAT) System: Experimental Aspects, *Journal of Vibration and Acoustics*, 129, pp. 209-216.

[14] Savaresi, S., 2008, Semi-Active Control Strategies for High-Performance Motorcycles. Proceedings of the 17th IFAC World Congress, 2008, 4689-4694.

[15] Spelta, C., Savaresi, S., & Fabbri, L. (n.d.). Experimental analysis of a motorcycle semi-active rear suspension. Control Engineering Practice, 1239-1250.

[16] Storr, W., 2013, Butterworth Filter Design and Low Pass Butterworth Filters. Retrieved October 12, 2015, from http://www.electronics-tutorials.ws/filter/filter_8.html

[17] Strydom, A., 2013, Controllable Suspension Design Using Magnetorheological Fluid, Master's Thesis, University of Pretoria, South Africa.

[18] Trevitt, A., 2014, Semi-Active Suspension. Retrieved October 12, 2015, from http://www.sportrider.com/tech/semi-active-suspension

[19] Weiss, K. D., Duclos, T. G., Carlson, J. D., Chrzan, M. J., Margida, A. J., 1993, High strength magneto – and electro – rheological fluids, *Society of Automotive Engineers*, 932451.

[20] Wereley, N. M., 2008, Shock Isolation Systems Using Magnetorheological Dampers, *Journal of Vibration and Acoustics*, 130, pp. 1-6.

[21] Wereley, N. M., 2014, Magnetorheology: Advances and Applications, Royal Society of Chemistry, RSC Smart Materials, Cambridge, UK. DOI: 10.1039/9781849737548.

[22] Yu, M., 2006, Study on MR Semi-active Suspension System and its Road Testing, *Journal of Intelligent Material Systems and Structures*, 17, pp. 801-806.

APPENDIX A

MATLAB Programs

Appendix A provides all the MATLAB programs developed and used for this study.

The following MATLAB program has been used to analyze and plot the data collected from the tensile testing, and subsequently used to characterize the damper.

```
data_1 = xlsread('Data_1');
t1 = data_1(:,1); % time in seconds
x1 = data_1(:,2); % displacement in mm
xdot1=diff(x1)/0.1;
xdot1=[0; xdot1];
f1 = data_1(:,3); % force in N (also called kgf)

figure, plot(x1,f1),grid,ylim([0 20])
xlabel('Displacement (mm)'), ylabel('Force (N)')
title('Damper Characteristics - 0A')
figure, scatter(xdot1,f1),grid
xlabel('Velocity (mm/s)'), ylabel('Force (N)')
title('Damper Characteristics - 0A')

data_2 = xlsread('Data_2');
t2 = data_2(:,1); % time in seconds
x2 = data_2(:,2); % displacement in mm
xdot2=diff(x2)/0.1;
xdot2=[0; xdot2];
f2 = data_2(:,3); % force in N

figure, plot(x2,f2),grid,ylim([0 20])
xlabel('Displacement (mm)'), ylabel('Force (N)')
title('Damper Characteristics - 0.5A')
figure, scatter(xdot2,f2),grid
xlabel('Velocity (mm/s)'), ylabel('Force (N)')
title('Damper Characteristics - 0.5A')

data_3 = xlsread('Data_3');
t3 = data_3(:,1); % time in seconds
x3 = data_3(:,2); % displacement in mm
xdot3=diff(x3)/0.1;
xdot3=[0; xdot3];
f3 = data_3(:,3); % force in N

figure, plot(x3,f3),grid,ylim([0 20])
xlabel('Displacement (mm)'), ylabel('Force (N)')
title('Damper Characteristics - 1.5A')
figure, scatter(xdot3,f3),grid
xlabel('Velocity (mm/s)'), ylabel('Force (N)')
```

```
title('Damper Characteristics - 1.5A')


data_4 = xlsread('Data_4');
t4 = data_4(:,1); % time in seconds
x4 = data_4(:,2); % displacement in mm
xdot4=diff(x4)/0.1;
xdot4=[0; xdot4];
f4 = data_4(:,3); % force in N

figure, plot(x4,f4),grid,ylim([0 20])
xlabel('Displacement (mm)'), ylabel('Force (N)')
title('Damper Characteristics - 1A')
figure, scatter(xdot4,f4),grid
xlabel('Velocity (mm/s)'), ylabel('Force (N)')
title('Damper Characteristics - 1A')

figure,plot(x1,f1,x2,f2,x4,f4,x3,f3,'LineWidth',2),grid,ylim([0 20])
legend('0A','0.5A','1A','1.5A')
xlabel('Displacement (mm)'), ylabel('Force (N)')
title('Damper Characteristics')
```

The following MATLAB program provides an example of the post-processing, filtering, FFT, plotting, and analysis that has been performed on the two channel data testing after collecting the accelerometer data.

```
% Data - 5-100 Hz

aa=xlsread('name of excel file');

aa_base=aa(:,2)/10;
[B,A] = butter(4,105/800,'low');
a_base=filter(B,A,aa_base);
[B,A] = butter(4,1/800,'high');
a_base=filter(B,A,a_base);

rms_b00=norm(a_base)/sqrt(length(a_base)-1)
max_b00=max(abs(a_base))

aa_payload=aa(:,3)/10;
[B,A] = butter(4,105/800,'low');
a_payload=filter(B,A,aa_payload);
[B,A] = butter(4,1/800,'high');
a_payload=filter(B,A,a_payload);

rms_p00=norm(a_payload)/sqrt(length(a_payload)-1)
max_p00=max(abs(a_payload))

figure,plot(aa(:,1),abs(a_base),'g',aa(:,1),abs(a_payload),'r'),grid
legend('Base','Payload'),xlabel('Time (s)'), ylabel('Acceleration (g)')
```

```
title('Title of Plot')
xlim([5 240])

Fs=1600;
L=length(a_base);
y_b=a_base;
NFFT=2^nextpow2(L);
y_bf=fft(y_b,NFFT)/L;
f_b=Fs/2*linspace(0,1,NFFT/2+1);
rms_bf=norm(y_bf)/sqrt(length(y_bf)-1)

L=length(a_payload);
y_p=a_payload;
NFFT=2^nextpow2(L);
y_pf=fft(y_p,NFFT)/L;
f_p=Fs/2*linspace(0,1,NFFT/2+1);
rms_pf=norm(y_pf)/sqrt(length(y_pf)-1)

figure,semilogx(f_b,2*abs(y_bf(1:NFFT/2+1)),'g')
hold on
semilogx(f_p,2*abs(y_pf(1:NFFT/2+1)),'r'),grid
legend('Base','Payload'),xlabel('Frequency (Hz)'),ylabel('Frequency
Response')
xlim([1 100])

figure,plot(f_b,2*abs(y_bf(1:NFFT/2+1)),'g')
hold on
plot(f_p,2*abs(y_pf(1:NFFT/2+1)),'r'),grid
legend('Base','Payload'),xlabel('Frequency (Hz)'),ylabel('Frequency
Response')

figure, scatter(a_base(1:10000),a_payload(1:10000)),grid
xlim([-0.1 0.1]),ylim([-0.1 0.1])
xlabel('Base acceleration (g)'),ylabel('Payload acceleration (g)')
```

The following MATLAB program provides an example of the post-processing, filtering, FFT, plotting, and analysis that has been performed on the three channel data testing after collecting the accelerometer data.

```
% Data - 5-100 Hz 3 Channel

aa=xlsread('Title of excel file');

aa_base=aa(:,2)/10;
[B,A] = butter(4,105/800,'low');
a_base=filter(B,A,aa_base);
[B,A] = butter(4,1/800,'high');
a_base=filter(B,A,a_base);
```

```
rms_b00=norm(a_base)/sqrt(length(a_base)-1)
max_b00=max(abs(a_base))

aa_foot=aa(:,3)/10;
[B,A] = butter(4,105/800,'low');
a_foot=filter(B,A,aa_foot);
[B,A] = butter(4,1/800,'high');
a_foot=filter(B,A,a_foot);

rms_f00=norm(a_foot)/sqrt(length(a_foot)-1)
max_f00=max(abs(a_foot))

aa_damper=aa(:,4)/10;
[B,A] = butter(4,105/800,'low');
a_damper=filter(B,A,aa_damper);
[B,A] = butter(4,1/800,'high');
a_damper=filter(B,A,a_damper);

rms_d00=norm(a_damper)/sqrt(length(a_damper)-1)
max_d00=max(abs(a_damper))

figure,plot(aa(:,1),abs(a_base),'g',aa(:,1),abs(a_damper),'b',aa(:,1),abs(a_f
oot),'r'),grid
legend('Base','Damper','Foot Peg'),xlabel('Time (s)'), ylabel('Acceleration
(g)')
title('title of plot')
xlim([5 240])

Fs=1600;
L=length(a_base);
y_b=a_base;
NFFT=2^nextpow2(L);
y_bf=fft(y_b,NFFT)/L;
f_b=Fs/2*linspace(0,1,NFFT/2+1);
rms_bf=norm(y_bf)/sqrt(length(y_bf)-1)

L=length(a_foot);
y_f=a_foot;
NFFT=2^nextpow2(L);
y_ff=fft(y_f,NFFT)/L;
f_f=Fs/2*linspace(0,1,NFFT/2+1);
rms_ff=norm(y_ff)/sqrt(length(y_ff)-1)

L=length(a_damper);
y_d=a_damper;
NFFT=2^nextpow2(L);
y_df=fft(y_d,NFFT)/L;
f_d=Fs/2*linspace(0,1,NFFT/2+1);
rms_df=norm(y_df)/sqrt(length(y_df)-1)

figure,semilogx(f_b,2*abs(y_bf(1:NFFT/2+1)),'g')
hold on
semilogx(f_d,2*abs(y_df(1:NFFT/2+1)),'b')
hold on
semilogx(f_f,2*abs(y_ff(1:NFFT/2+1)),'r'),grid
```

```
legend('Base','Damper','Foot Peg'),xlabel('Frequency (Hz)'),ylabel('Frequency
Response')
xlim([1 100])

figure,plot(f_b,2*abs(y_bf(1:NFFT/2+1)),'g')
hold on
plot(f_d,2*abs(y_df(1:NFFT/2+1)),'b')
hold on
plot(f_f,2*abs(y_ff(1:NFFT/2+1)),'r'),grid
legend('Base','Damper','Foot Peg'),xlabel('Frequency (Hz)'),ylabel('Frequency
Response')

figure, scatter(a_base(1:10000),a_foot(1:10000)),grid
xlim([-0.1 0.1]),ylim([-0.1 0.1])
xlabel('Base acceleration (g)'),ylabel('Foot Peg acceleration (g)')

figure, scatter(a_base(1:10000),a_damper(1:10000)),grid
xlim([-0.1 0.1]),ylim([-0.1 0.1])
xlabel('Base acceleration (g)'),ylabel('Damper acceleration (g)')
```

APPENDIX B

Specifications and Data Sheets

Appendix B provides the specification sheets for the main equipment used during this research. The specification sheets for the dampers and the accelerometers used are included for reference.

RD-8040-1 and RD-8041-1 Dampers

Description

LORD RD-8040-1 (short stroke) and RD-8041-1 (long stroke) dampers are compact, magneto-rheological (MR) fluid dampers suitable for industrial suspension applications. Continuously variable damping is controlled by the increase in yield strength of the MR fluid in response to magnetic field strength.

Features and Benefits

Fast Response Time – responds in less than 15 milliseconds to changes in the magnetic field.

Easy to Use – provides simple electronics and straight forward controls.

Durable – provides excellent long term stability.

Storage

Dampers should be stored at -40 to +100°C (-40 to +212°F).

The RD-8040-1 and RD-8041-1 dampers are monotube shocks containing high-pressure nitrogen gas (300 psi). Handle with care and do not heat or puncture body.

Electrical Properties*

Input Current, Amp	
Continuous for 30 seconds	1 max
Intermittent	2 max
Input Voltage, Volt	12 DC
Resistance, ohms	
@ ambient temperature	5
@ 71°C (160°F)	7

*Data is typical and not to be used for specification purposes.

Typical Properties*

	RD-8040-1	RD-8041-1
Stroke, mm (in)	55 (2.17)	74 (2.91)
Extended Length, mm (in)	208 (8.2)	248 (9.76)
Body Diameter, mm (in)	42.1 (1.66) max	42.1 (1.66) max
Shaft Diameter, mm (in)	10 (0.39)	10 (0.39)
Tensile Strength, N (lbf)	8896 (2000) max	8896 (2000) max
Damper Forces, N (lbf)		
Peak to Peak		
5 cm/sec @ 1 A	>2447 (>550)	>2447 (>550)
20 cm/sec @ 0 A	<667 (<150)	<667 (<150)
Operating Temperature, °C (°F)	71 (160) max	71 (160) max

*Data is typical and not to be used for specification purposes.

LORD
Ask Us How™

Typical Force vs. Velocity

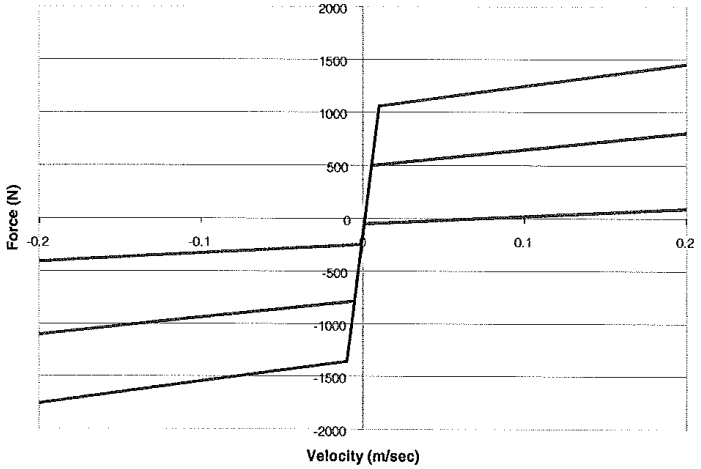

Offset at origin is due to gas precharge required for temperature compensation and to prevent cavitation.

LORD provides valuable expertise in adhesives and coatings, vibration and motion control, and magnetically responsive technologies. Our people work in collaboration with our customers to help them increase the value of their products. Innovative and responsive in an ever-changing marketplace, we are focused on providing solutions for our customers worldwide ... Ask Us How.

LORD Corporation
World Headquarters
111 Lord Drive
Cary, NC 27511-7923
USA

Customer Support Center (in United States & Canada)
877 ASK LORD (275 5673)

www.lord.com

For a listing of our worldwide locations, visit LORD.com/locations.

LORD
Ask Us How™

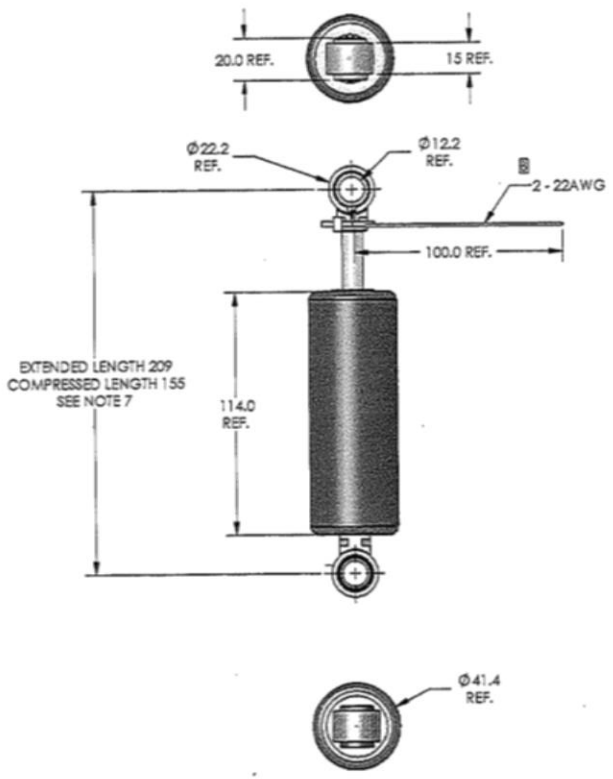

REV	DESCRIPTION	DATE	DR
A	PCN RD-1005-3-A	10/24/2001	JK
B	PCN RD-1005-3-B	1/20/2006	SL

NOTES:

1. ALL DIMENSIONS ARE REFERENCE DIMENSIONS.
2. FOR INSTALLATION ON 12mm SHAFT.
3. ELECTRICAL SPECIFICATION:
   - INPUT CURRENT = 1AMP MAX. CONTINUOUS; = 2AMPS MAX. INTERMITTENT
   - INPUT VOLTAGE = 12VDC
   - RESISTANCE = 5 Ω AT AMBIENT TEMPERATURE
   - RESISTANCE = 7 Ω AT 71°C (160°F)
4. DAMPER FORCES: (PEAK TO PEAK)
   - 0.05 M/S AT 1 AMP = > 2224 N (500 POUNDS)
   - 0.20 M/S AT 0 AMP = <667 N (150 POUNDS)
5. MECHANICAL SPECIFICATIONS
   - MAXIMUM TENSILE LOAD = 4448 N (1000 POUNDS)
   - MAXIMUM OPERATING TEMPERATURE = 71°C (160°F)
   - STORAGE TEMPERATURE LIMITS: = -40°C TO 100°C (-40°F TO 212°F)
6. DURABILITY
   DAMPER FORCE (PEAK TO PEAK) @ 0.20 M/S @ 0 AMPS =<890 N (200 POUNDS) - AFTER 2 MILLION CYCLES @ +/- 12.5mm, 2 HERTZ WITH INPUT CURRENT VARYING BETWEEN 0 AND 0.8 AMPS.
7. DESIGN NOTE:
   DAMPER STROKE MUST BE LIMITED WITHIN THE SPECIFIED STROKE RANGE. ALLOW A MINIMUM SAFETY CLEARANCE OF 6mm OR DAMPER DAMAGE MAY RESULT.

DRAWING RELEASE TYPE UNLESS OTHERWISE SPECIFIED:

EXPERIMENTAL –

PROTOTYPE –

PRODUCTION X

FINAL ASSY –

WEIGHT:
REF. DWG

LORD®
Material Division
406 Gregson Dr.
Cary, N. C. 27511-7900

DR. S. H. LAND 1/20/2006
CHK.
ENG APPR.
MFG. APPR.
Q.A.

TITLE: MR DAMPER ASSY. COMMERCIAL SPEC.

SIZE B | DWG. NO. RD-1005-3 Sht 1 of 1 | REV B

1/27/2006 3:39 PM

OPERATING INSTRUCTIONS

MODELS 3019A & 3019A1 HIGH FREQUENCY LIVM ACCELEROMETERS

INTRODUCTION

Model 3019A has a 1/4-28 integral mounting stud. Model 3019A1 has a 10-32 integral stud. All other specifications are similar.

Series 3019A are miniature high frequency quartz accelerometers with built in impedance converting amplifier. These versatile instruments utilize pure Alfa quartz crystals in compression mode to generate voltage signals exactly analogous to input accelerations including shock and vibration.

An internal MOSFET integrated circuit (IC) amplifier operating as a source follower, converts the very high impedance level signals from the quartz crystals to a low impedance voltage mode signal which is able to drive long cables and feed directly into many types of readout instruments. Output signals are directly in units of mV/g.

The miniature on-board amplifier requires 2 to 20 mA of constant current supplied by special LIVM power units with compliance voltages from +18 to +30 Volts DC. Sensor power and signal are conducted over a single pair of wires allowing the use of inexpensive coaxial cable for system interconnections. Even less expensive twin lead cable may also be used.

Voltage mode systems such as described here feature fixed sensitivity signals, unaffected by cable length. A calibration certificate, traceable to NIST is provided to define the exact sensitivity and frequency response of each instrument.

The sensitivity of Series 3019A is 10.0 mV/g, ± 5% @ 100 Hz and the frequency response is ± 5% from 1 Hz to 10 kHz.

Series 3019A features ground isolated construction, i.e., the mounting surface is electrically isolated from the case (electrical ground) of the instrument. This means that if the test surface is at an elevated electrical potential from power ground, this will have no effect on the sensor signal. This feature precludes annoying "Ground Loops".

Series 3019A are truly hermetically sealed instruments. All joints are TIG welded and the connector is a glass to metal hermetic sealed design.

DESCRIPTION

Refer to Fig. 1 and Outline/Installation drawings 127-3019A & 127-3019A1)

Both models utilize an upright, compression mode quartz element to maximize the mechanical coupling from mounting base to quartz seismic element for best high frequency fidelity. A special strain isolation base minimizes the unwanted effects of base strain on the accelerometer signal. By careful design and fabrication techniques, the excellent high frequency response and low base strain are optimized.

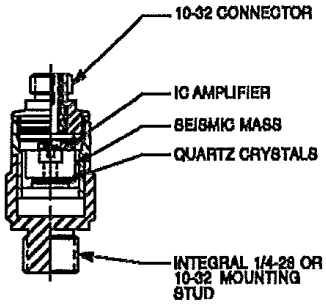

Figure 1 Cross section series 3019A

The highly preloaded quartz crystals coupled to a dense tungsten seismic mass ensure excellent linearity over the entire dynamic range with minimal distortion.

The integral MOSFET IC amplifier has been proven dependable to 100,000 g's shock, providing high reliability.

The IC amplifier operates from constant current type power units (many types are available from Dytran) and may be supplied with from 2 to 20 mA of current, depending upon the length of cable being driven by the sensor. The current is supplied to the source terminal of the sensor amplifier (see Fig. 2) and this point is normally biased at approximately +10 Volts DC.

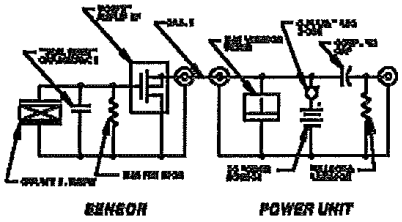

Figure 2 System Schematic

The DC bias voltage of the sensor amplifier is blocked by the 10 uF coupling capacitor in the power unit and only the dynamic signal from the sensor is allowed to pass to the readout instrument.

Referring to Fig. 2, within the accelerometer, the resistor from the gate of the MOSFET to ground serves to bias the amplifier at its proper operating point and it also establishes the low frequency response of the sensor by setting the discharge time constant (TC) of the accelerometer. This resistor and the total shunt capacitance C across it (the crystal, gate and stray capacitance) set the TC which in turn sets the low frequency response as follows:

$$f_{-3db} = \frac{.16}{RC} \qquad \text{(Eq. 1)}$$

where:

f_{-3db} = The lower -3db frequency (Hz)

R = bias resistor value (Ohms)

C = total shunt capacitance across bias resistor

The product RC is also known as discharge Time Constant or TC. Series 3019A has a TC of .5 seconds. Applying equation 1, the lower -3db frequency of Series 3019A is .32 Hz and the -5% frequency is 3 times the -3db frequency or .96 Hz.

Referring to Fig. 2, most Dytran power units feature a DC voltmeter which reads this bias voltage from the sensor and as such, serves as a very useful system trouble shooting tool. (For more information on this feature, refer to the paper "Low Impedance Voltage Mode (LIVM) Theory and Operation", included with this manual.

Dytran offers many types of current source power units to operate LIVM sensors like Series 3019A. These include the single channel battery operated Models 4102 and 4105, which supply fixed 2 mA of constant current, the line powered single channel model 4110, and the four channel model 4114, both of which feature adjustable drive current. Also included are many types of other multiple channel units with 6, 12 and 16 sensor channels.

INSTALLATION

Refer to Outline/Installation drawing 127-3019A or drawing 127-3019A1 for this section.

To install either Model, it is necessary to select or prepare a smooth, flat mounting area at least .375 in diameter. The surface should be flat to .001 TIR and may be prepared by various machining methods such as spotfacing, grinding, turning, etc. if required.

It is important that the accelerometer base be in intimate contact with the mounting surface for best high frequency response and for faithful reproduction of the calibrated sensitivity over all frequencies.

For Model 3019A, at the center of the selected mounting area, drill and tap a 1/4-28, UNF-2B mounting hole with minimum thread depth of .250. (Be careful to ensure that the drilled hole is perpendicular to the mounting surface to within ±1°.) For Model 3019A1, drill and tap a 10-32 UNF-2b mounting hole with a minimum thread depth of .250.

After this operation, clean the area thoroughly to remove all traces of oil, machining chips and burrs which could preclude intimate contact between mounting surfaces.

Coat one of the mating surfaces with a thin layer of silicone grease, then thread the Series 3019A or A1 integral stud into the mounting hole so that the mounting surfaces just meet. Inspect the mating surfaces to see that they contact squarely, inspecting for chips which may have become lodged between the mating surfaces. If the contact looks square, proceed to torque the sensor down with 20 to 25 lb-inches of torque, preferably using a torque wrench with a 3/8 in. deep socket gripping on the 3/8 in. hex of the case.

Connect the accelerometer to the power unit using Model 6010AXX or 6011AXX coaxial cable. Model 6010A is used when the power unit

has 10-32 input connectors and Model 6011A is used when the power unit has BNC jack input connectors. Carefully tighten the 10-32 knurled nut at the sensor, by hand to ensure a secure connection. Do not use pliers on this cable nut as this may damage the cable or sensor connector.

Under high shock or high vibration conditions, it may be discovered that the cable nut has become loose and is causing erratic readings. Under these conditions, it may be advisable to use a mild thread locking agent such as Loctite® on the threads of the 10-32 connector when re-installing the cable.

Connect the "Output" jack of the power unit to the readout instrument (oscilloscope, recorder, meter, etc.) and proceed with the measurement.

MONITOR METER

Refer to the section "Monitor Meter" in the paper, "Low Impedance Voltage Mode (LIVM) Theory and Operation", supplied with this manual for a guide to using the monitor meter on the front of most Dytran power units as a handy trouble shooting tool for LIVM systems.

MAINTENANCE AND REPAIR

The sealed construction of the 3019A Series precludes most maintenance other than that necessary to maintain a smooth mounting surface at the accelerometer base mounting surface.

Periodically inspect the mounting base surface for nicks or deep scratches, gouges and other imperfections which could prevent intimate contact between mating surfaces. If surface imperfections are discovered, you may want to consider returning the unit to the factory for a dressing of the mounting surface.

The electrical connector may be cleaned if necessary, with a cloth or paper wipe dipped in Freon ® or alcohol. After this operation, it may be beneficial to bake the sensor out in a drying oven at 200 to 250 °F for an hour or so. **Never higher than +300°F!**

Should a problem arise with the sensor, contact the factory for assistance. If the instrument must be returned for evaluation, you will be issued a **Returned Material Authorization** (RMA) number to help guide the instrument through the evaluation process. Please do not return any instrument or power unit to the factory without first obtaining an RMA number.

We will not proceed with repairs without first notifying you of charges (if any) and obtaining your approval. There is no charge for evaluation of the instrument.

CAUTIONS

1) Do not store or use Series 3019A above +300°F.

2) For best frequency response, measure the mounting torque, don't guess.

3) Never connect the sensor to a power source (battery or power supply) which does nor have current limiting, 20 mA MAX! This will immediately destroy the integral IC amplifier.

4) Do not attempt to measure the resistance at the sensor connector as many ohmmeters supply too much current for the internal IC and may destroy it.

REV	ECN	DESCRIPTION	BY/DATE	CHK	APPR
A	10476	REMOVED WELD GROOVES	NC/11-5-13		

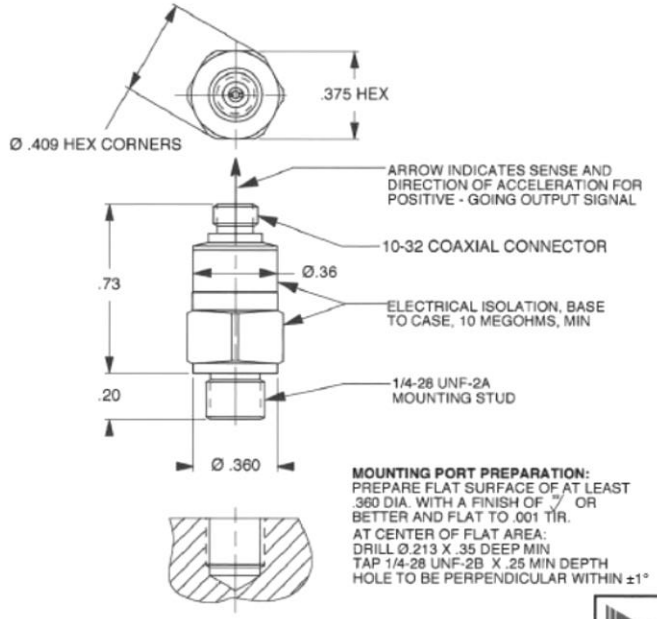

MOUNTING PORT PREPARATION:
PREPARE FLAT SURFACE OF AT LEAST .360 DIA. WITH A FINISH OF ▽ OR BETTER AND FLAT TO .001 TIR.
AT CENTER OF FLAT AREA:
DRILL Ø.213 X .35 DEEP MIN
TAP 1/4-28 UNF-2B X .25 MIN DEPTH
HOLE TO BE PERPENDICULAR WITHIN ±1°

3. MATERIAL: 300 SERIES STAINLESS STEEL.
2. WEIGHT: 8 GRAMS.
1. RECOMMENDED MOUNTING TORQUE ON 3/8 IN. HEX: 20 TO 25 LB.-INCHES.

DYTRAN INSTRUMENTS, INC. — CHATSWORTH, CA.

MASTER ONLY IF IN RED

SCALE 2X	DESIGN N.C.	DATE 6/2/98			
DRAWN N.C.	DATE 6/2/98	PART NO. MODEL 3019A			
CHECKED R.A.	DATE 6/2/98	MAT'L			REV A
APPROVED	DATE 6/2/98	NEXT ASSEMBLY	USED ON 3019A		

TITLE: **OUTLINE/INSTALLATION DRAWING, HIGH FREQUENCY ACCELEROMETER MODEL 3019A**

DWG NO. **127-3019A**

SHEET 1 OF 1